ARMY RESEARCH LABORATORY

Stress Wave and Damage Propagation in Transparent Laminates at Elevated Temperatures

by Elmar Straßburger

ARL-CR-639 **March 2010**

prepared by

Fraunhofer-Gesellschaft zur Förderung der angewandten Forschung e.V.
Hansastraße 27 c, 80686 München, Germany

under contract

W911NF-08-1-2006

NOTICES

Disclaimers

The findings in this report are not to be construed as an official Department of the Army position unless so designated by other authorized documents.

Citation of manufacturer's or trade names does not constitute an official endorsement or approval of the use thereof.

Destroy this report when it is no longer needed. Do not return it to the originator.

Army Research Laboratory
Aberdeen Proving Ground, MD 21005-5069

ARL-CR-639 **March 2010**

Stress Wave and Damage Propagation in Transparent Laminates at Elevated Temperatures

Elmar Straßburger
Fraunhofer-Gesellschaft zur Förderung der angewandten Forschung e.V.

prepared by

Fraunhofer-Gesellschaft zur Förderung der angewandten Forschung e.V.
Hansastraße 27 c, 80686 München, Germany

under contract

W911NF-08-1-2006

REPORT DOCUMENTATION PAGE	Form Approved OMB No. 0704-0188

1. REPORT DATE *(DD-MM-YYYY)*	2. REPORT TYPE	3. DATES COVERED (From - To)
March 2010	Final	November 2007–November 2008

4. TITLE AND SUBTITLE
Stress Wave and Damage Propagation in Transparent Laminates at Elevated Temperatures

5a. CONTRACT NUMBER
W911NF-08-1-2006

5b. GRANT NUMBER

5c. PROGRAM ELEMENT NUMBER

6. AUTHOR(S)
Elmar Straßburger

5d. PROJECT NUMBER

5e. TASK NUMBER

5f. WORK UNIT NUMBER

7. PERFORMING ORGANIZATION NAME(S) AND ADDRESS(ES)
Fraunhofer-Gesellschaft zur Förderung der angewandten Forschung e.V.
Hansastraße 27 c, 80686 München, Germany

8. PERFORMING ORGANIZATION REPORT NUMBER
E 13/09

9. SPONSORING/MONITORING AGENCY NAME(S) AND ADDRESS(ES)
U.S. Army Research Laboratory
ATTN: RDRL-WMM-D
Aberdeen Proving Ground, MD 21005-5069

10. SPONSOR/MONITOR'S ACRONYM(S)
ARL

11. SPONSOR/MONITOR'S REPORT NUMBER(S)
ARL-CR-639

12. DISTRIBUTION/AVAILABILITY STATEMENT
Approved for public release; distribution is unlimited.

13. SUPPLEMENTARY NOTES

14. ABSTRACT

A series of studies has been conducted to visualize damage initiation and propagation in transparent armor materials like Starphire (a registered trademark of PPG Industries, Pittsburgh, PA) soda-lime glass, borosilicate glass, fused silica, and the transparent ceramic AlON. Since transparent armor consists of glass laminates with polymer interlayer and backing, the influence of interlayer type and thickness on damage propagation was also examined.

The so-called Edge-on Impact method was applied to visualize stress wave and damage propagation in the previous sets of tests. Two different optical configurations were employed. A regular transmitted light shadowgraph setup was used to observe wave and damage propagation, and a modified configuration, where the specimens were placed between crossed polarizers, and the photoelastic effect was utilized to visualize the stress waves. Pairs of impact tests at approximately equivalent velocities were carried out in transmitted plane (shadowgraphs) and crossed polarized light.

The focus of this study was on the investigation of the influence of a layer of strengthened glass or glass ceramic in a laminate target and the influence of elevated temperatures on wave and damage propagation.

15. SUBJECT TERMS
edge-on impact, visualization, stress waves, laminates

16. SECURITY CLASSIFICATION OF:			17. LIMITATION OF ABSTRACT	18. NUMBER OF PAGES	19a. NAME OF RESPONSIBLE PERSON
a. REPORT	b. ABSTRACT	c. THIS PAGE			Parimel Patel
Unclassified	Unclassified	Unclassified	UU	58	19b. TELEPHONE NUMBER (*Include area code*) (410) 306-0744

Standard Form 298 (Rev. 8/98)
Prescribed by ANSI Std. Z39.18

Contents

List of Figures

List of Tables

Acknowledgments

The research reported in this document has been made possible through the support and sponsorship of the U.S. Government through its European Research Office of the U.S. Army.

1. Introduction

A series of studies has been conducted to visualize damage initiation and propagation in transparent armor materials like Starphire* soda-lime glass, borosilicate glass, fused silica, and the transparent ceramic AlON.[1] Since transparent armor consists of glass laminates with polymer interlayer and backing, the influence of interlayer type and thickness on damage propagation was also examined.[2] Thick glass-polymer laminates used as transparent armor in vehicles can heat up through intensive sunlight, which can significantly influence the performance of the armor. Therefore, the influence of elevated temperatures on the stress wave and damage propagation in a transparent laminate was examined in this study.

The so-called Edge-on Impact (EOI) method was applied in order to visualize stress wave and damage propagation in the previous sets of tests. Two different optical configurations were employed. A regular transmitted light shadowgraph setup was used to observe wave and damage propagation and a modified configuration, where the specimens were placed between crossed polarizers, and the photoelastic effect was utilized to visualize the stress waves. Pairs of impact tests at approximately equivalent velocities were carried out in transmitted plane (shadowgraphs) and crossed polarized light.

The objectives of the present study are as follows:

- To determine the influence of elevated temperatures on stress wave and damage propagation in glass laminates.
- To analyze the development of the damaged areas quantitatively, including previous sets of tests.
- To complement the test series with glass laminates that include a layer of strengthened glass.

The results of the analyses from previous tests with Starphire laminates with respect to the damaged areas have been presented in the 1st Interim Report.[3] This final report comprises the following:

*Starphire is a registered trademark of PPG Industries, Pittsburgh, PA.

[1]Straßburger, E. *High-Speed Photographic Study of Wave Propagation and Impact Damage in Transparent Aluminum Oxynitride (AlON)*; Final Report, contract no. N62558-04-P-6031, E 08/06; Ernst-Mach Institute: Efringen-Kirchen, Germany, February 2006.

[2]Straßburger, E. *High-Speed Photographic Study of Wave Propagation and Impact Damage in Transparent Laminates*; Final Report, contract no. N62558-05-P-0303, E 12/07; Ernst-Mach Institute: Efringen-Kirchen, Germany, February 2007.

[3]Straßburger, E. *Stress Wave and Damage Propagation in Transparent Laminates at Elevated Temperatures*; 1st Interim Report, contract no. W911NF-08-1-0006, E 22/08; Ernst-Mach Institute: Efringen-Kirchen, Germany, May 2008.

- Damaged area analyses from complementary baseline tests with Borofloat,* Starphire, two types of glass ceramic, and baseline data with an air gap between two layers of Starphire glass (section 3).
- Results from laminates that include an interlayer of strengthened glass or glass ceramic (section 4).
- Results from two-layer Starphire samples at elevated temperatures (section 5).

2. Experimental

The materials were tested in an EOI configuration, shown schematically in figure 1.

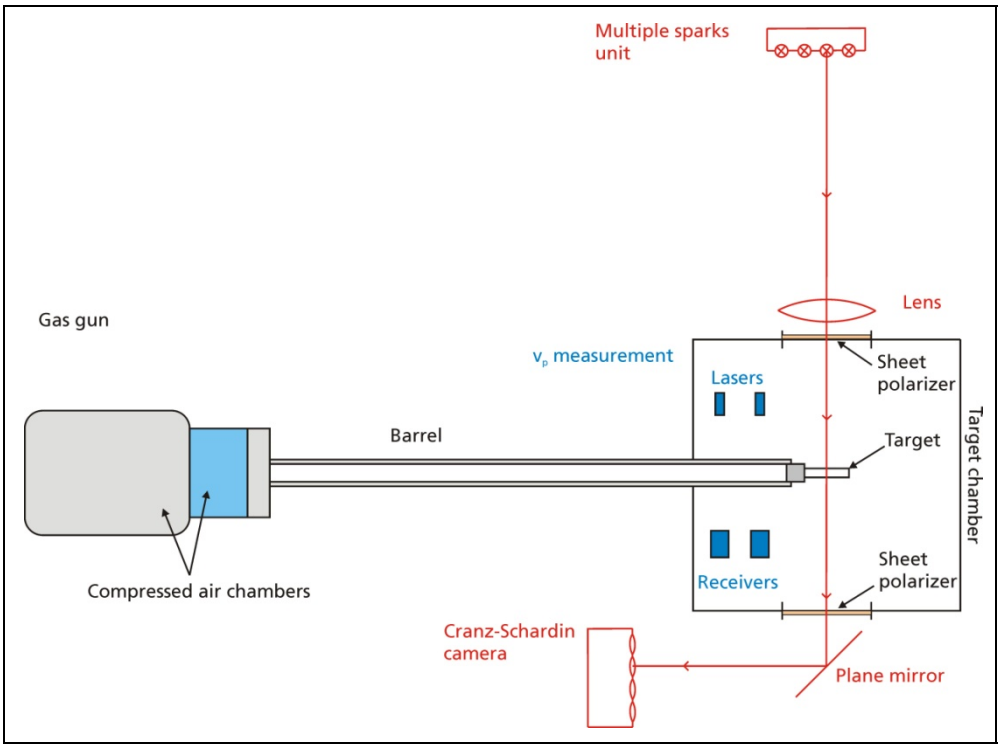

Figure 1. Schematic of EOI test setup.

Two types of projectiles were utilized for baseline tests to determine crack velocities, damage velocities, and wave propagation velocities in transparent materials—right-circular steel cylinders of 30-mm diameter and 53-g mass and steel spheres of 15.87-mm diameter and 16.2-g mass. With the steel cylinders, the nominal impact velocity was kept constant at about 400 m/s. A polycarbonate sabot was used to launch the steel spheres. Since the total mass of the sabot and

*Borofloat is a registered trademark of Schott Corporation.

steel sphere was less than the mass of the steel cylinder, the impact velocity was slightly higher and ranged from 420 to 440 m/s. Figure 2 shows a schematic of the steel cylinders and photograph of a spherical projectile with sabot. The fracture pattern generated by the spherical, diverging stress waves allows a measurement of the terminal crack velocity with good accuracy, whereas the damage pattern generated by the impact of the cylindrical projectile allows the measurement of damage velocities, determined by the nucleation of crack centers.

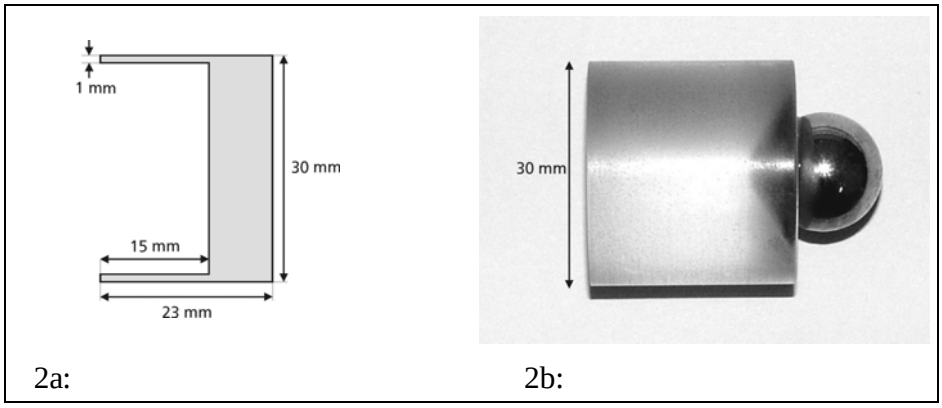

Figure 2. (a) Schematic of cylindrical steel projectile (cross section) and (b) photograph of spherical steel projectile with sabot.

For the simultaneous observation of the specimens from the side and top, an optical setup with two Cranz-Schardin cameras was utilized in all tests. Figure 3 shows a schematic of this optical configuration.

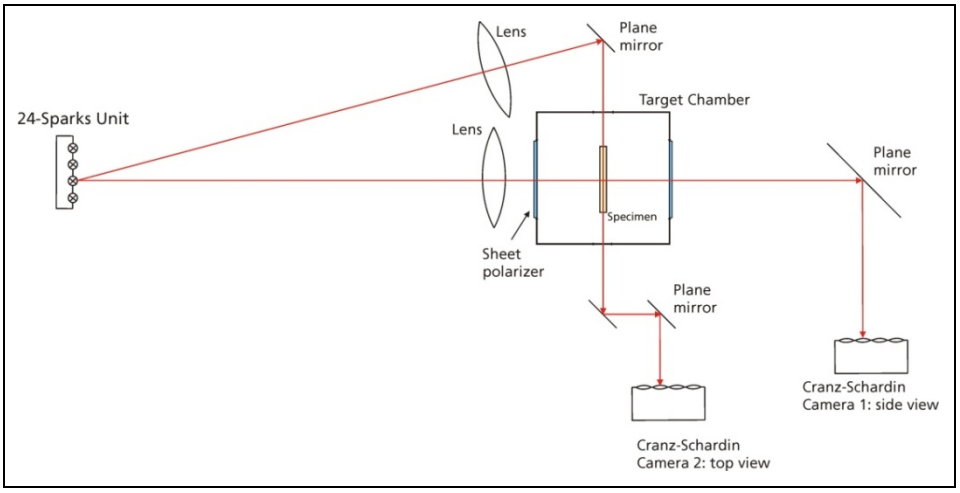

Figure 3. Schematic of the modified optical configuration.

3. Complementary Baseline Results

Complementary tests with Borofloat and Starphire glass were conducted, with extended time intervals of observation compared to previous tests to attain complete damage evolution curves for these materials. Especially with the spherical impactor, the damage evolution had only been observed up to about 40% of the damaged area in earlier experiments. Additionally, baseline damage evolution data of two glass ceramics were determined since these materials were also used as interlayer in laminated targets.

3.1 Borofloat

Two baseline tests were conducted with Borofloat glass, one with the cylindrical and one with the spherical projectile. Figures 4 and 5 each show a selection of eight high-speed photographs from these tests. The complete sets of high-speed photographs are shown in figures A-1 and A-2 of the appendix.

The corresponding damage evolution curves, which show the percentage of damaged area as a function of time, are depicted in figure 6. The data are shown, along with the results from previous base line tests, with a shorter time interval of observation.

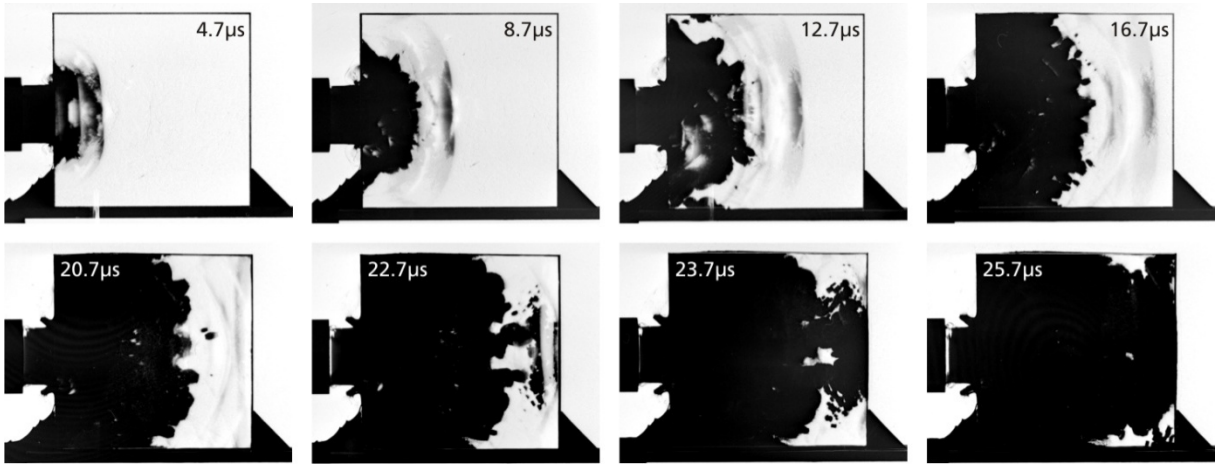

Figure 4. Selection of eight high-speed photographs from baseline test with Borofloat, cylindrical projectile, impact velocity 392 m/s, test no. 16591.

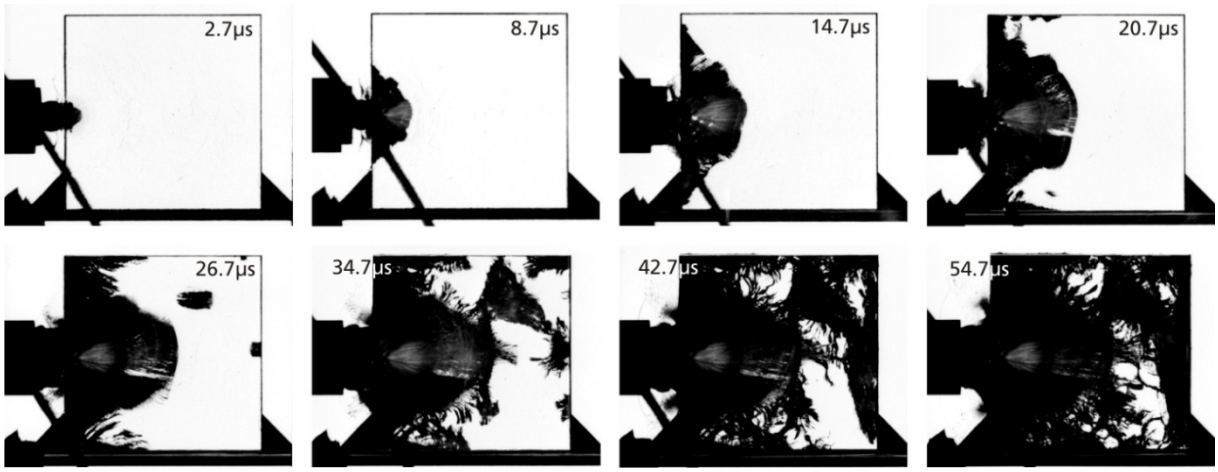

Figure 5. Selection of eight high-speed photographs from baseline test with Borofloat, spherical projectile, impact velocity 435 m/s, test no. 16594.

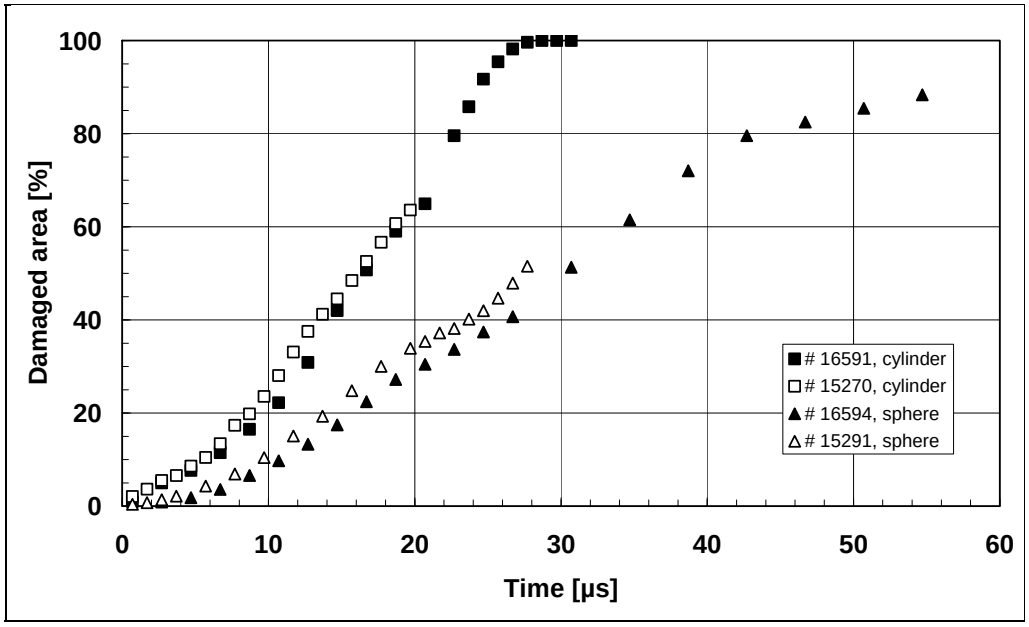

Figure 6. Damage evolution in Borofloat after impact of cylindrical and spherical projectile at ≈400 m/s.

The damage evolution curves in figure 6 show agreement between the actual baseline data and previous sets of data. Due to the formation of crack centers ahead of the coherent fracture, front damage propagates much faster under impact of the cylindrical projectile. In the test with the cylindrical projectile, the complete area of the Borofloat sample was damaged after 28 µs, whereas with the spherical projectile, 90% of damaged area was reached after 55 µs.

3.2 Starphire

One complementary test with a spherical projectile and extended time intervals was conducted with a Starphire specimen. Figure 7 shows a selection of eight high-speed photographs from this test. The complete set of high-speed photographs is shown in figure A-3 of the appendix.

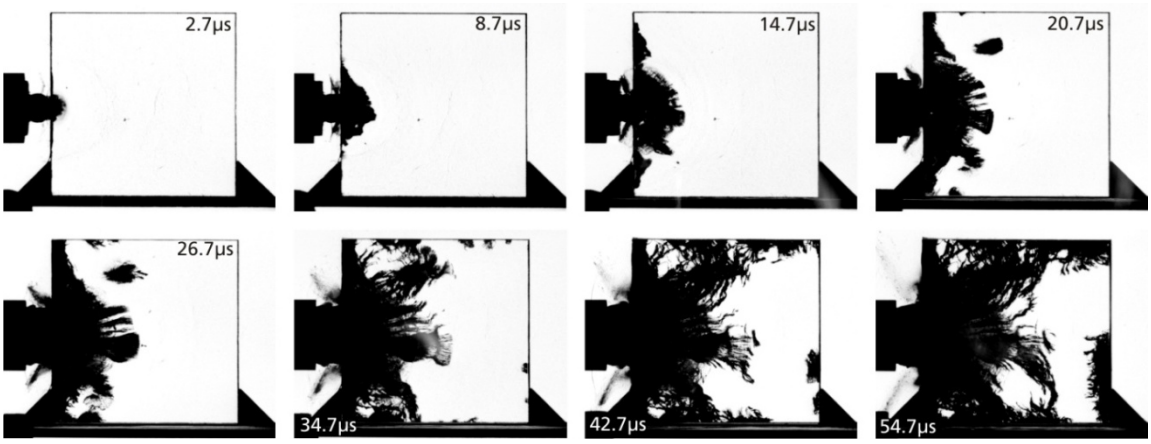

Figure 7. Selection of eight high-speed photographs from baseline test with Starphire, spherical projectile, impact velocity 432 m/s, test no. 16595.

It can be recognized from the selected high-speed photographs that Starphire damage evolution progresses slower compared to Borofloat. The quantitative analysis of the percent of damaged area yielded 62% after 55 µs with the Starphire, whereas 88% of damaged area was observed with the Borofloat specimen at the same time after impact. The damage evolution curve derived from the test with Starphire and the spherical projectile is plotted in figure 8, along with data from previous tests with spherical and cylindrical projectiles.

3.3 Glass Ceramics

Two types of glass ceramics were used as interlayer in laminate targets (see section 5). To obtain baseline data of damage evolution in these materials, one EOI test in a shadowgraph configuration was conducted with a cylindrical projectile for each material. The glass ceramics were from Schott and Corning. Figures 9 and 10 show a selection of eight high-speed photographs from the two tests. The complete sets of high-speed photographs are shown in figures A-4 and A-5 of the appendix.

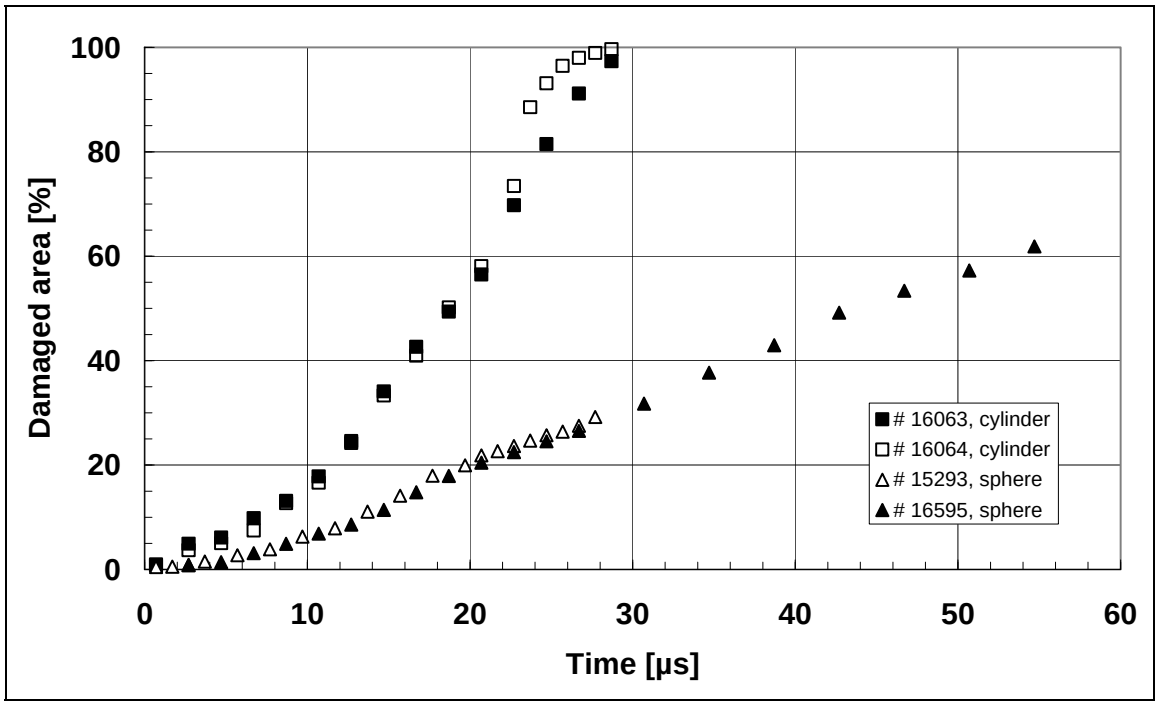

Figure 8. Damage evolution in Starphire after impact of cylindrical and spherical projectile at ≈400 m/s.

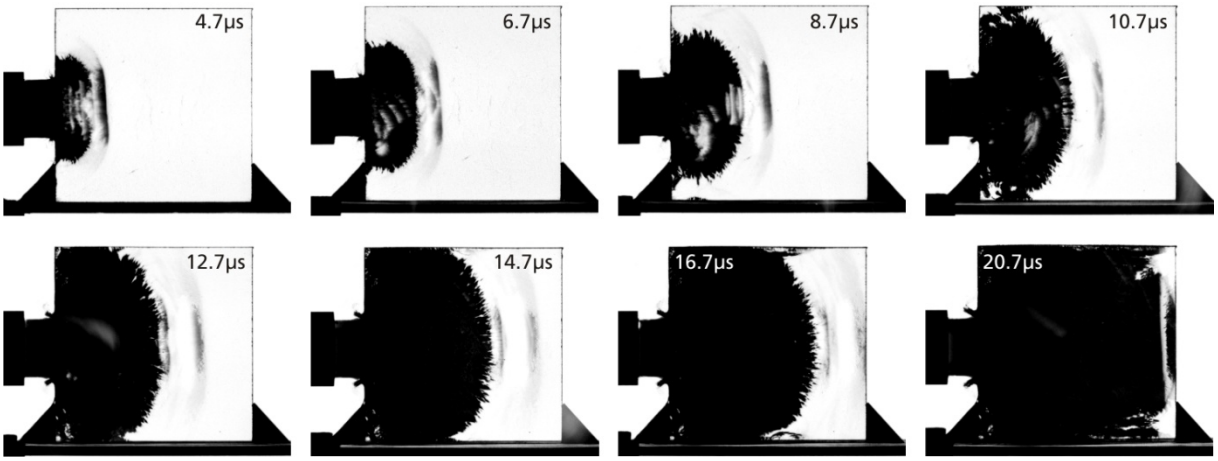

Figure 9. Selection of eight high-speed photographs from baseline test with Corning glass ceramic, cylindrical projectile, impact velocity 388 m/s, test no. 16592.

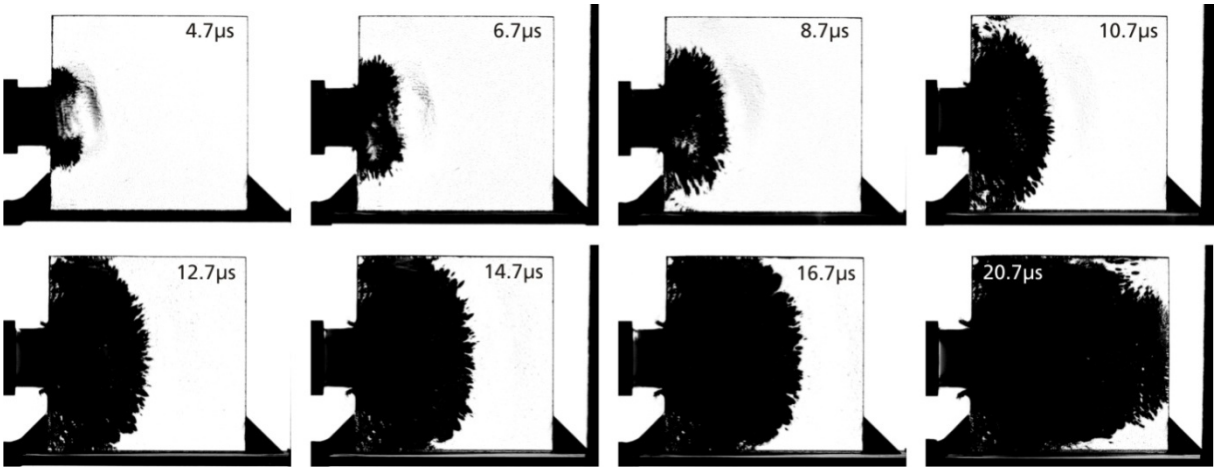

Figure 10. Selection of eight high-speed photographs from baseline test with Schott glass ceramic, cylindrical projectile, impact velocity 393 m/s, test no. 16593.

With both materials, a consistently growing coherent fracture front formed by a high number of uniformly distributed crack centers can be recognized. The Schott glass ceramic exhibits a slightly rougher fracture front, which seems to be due to a slightly lower density of crack centers.

The corresponding damage evolution curves are depicted in figure 11, along with data of Transarm glass ceramic from a previous set of tests.[4] With all three glass ceramics examined, the data in figure 11 demonstrate a very similar progression of the damage evolution.

4. Baseline Tests With Air Gap

Most of the two-layer laminate targets tested consisted of two 100- × 50-mm glass parts, which were joined together by polyurethane bonding layers of different types and thicknesses. The influence of the bonding layer on the transmission of stress waves from one glass layer to another was studied comprehensively.[2] The objective of the tests with an air gap between the glass layers was to study the effect of damage formation through particle impact on the second glass layer compared to damage initiation by stress wave transmission.

To measure the velocity of the glass fragments at the back of the first glass layer, one test was conducted with only one 100- × 50- × 9.4-mm specimen, which was impacted with a cylindrical projectile at 388 m/s. A selection of eight high-speed shadowgraphs is presented in figure 12. The complete set of high-speed photographs is shown in figure A-6 of the appendix.

[4]Straßburger, E. *Visualization of Wave and Damage Propagation in Transparent Armor Materials—Edge-On Impact Tests and Analysis*; Final Report, contract no. N62558-07-P-0331; E 13/08; Ernst-Mach Institute: Efringen-Kirchen, Germany, March 2008.

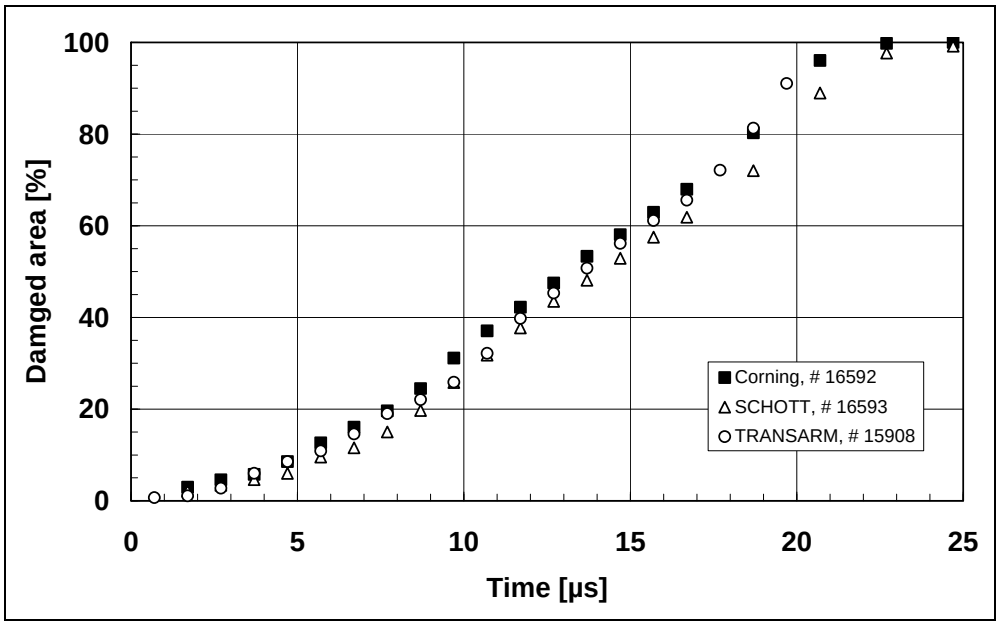

Figure 11. Damage evolution in glass ceramics after impact of a cylindrical projectile at ≈400 m/s.

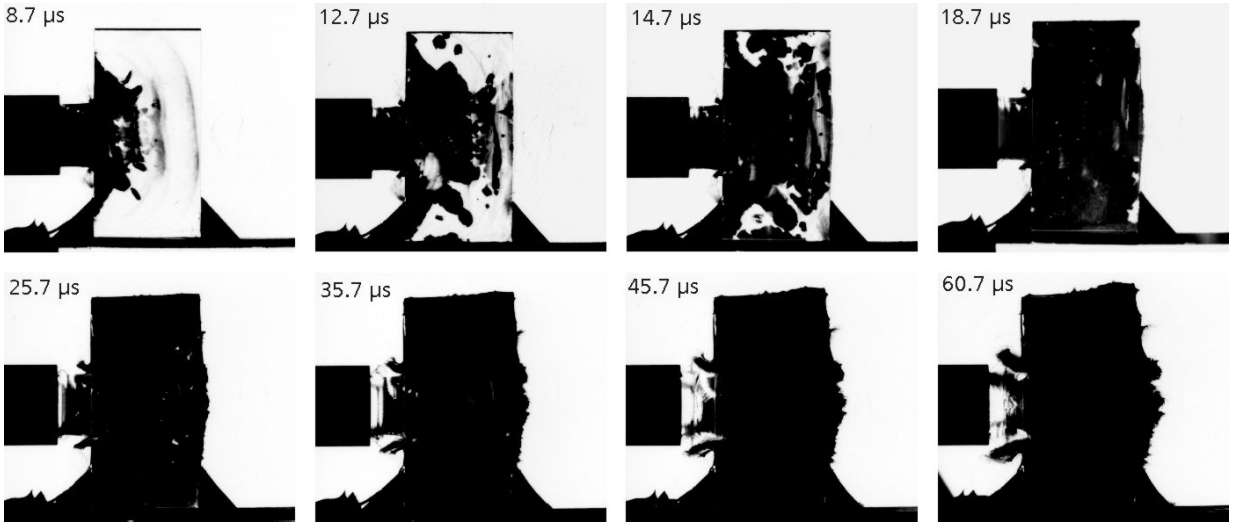

Figure 12. Selection of eight high-speed photographs from test with the 100- × 50-mm Starphire specimen, cylindrical projectile, impact velocity 388 m/s, test no. 16580.

The photographs in figure 12 demonstrate that the glass was already damaged at the rear side of the specimen about 13 µs after impact and a seeming deformation of the specimen had started after about 15 µs. The change of the specimen's contour at the rear side indicates that the glass is fragmented and particles are already moving at a high velocity. The path-time history of glass particles close to the center of the rear side of the specimen was determined from the

shadowgraphs. The position of the particles is plotted vs. time in figure 13. Linear regression of the data yielded an average velocity of 337 m/s.

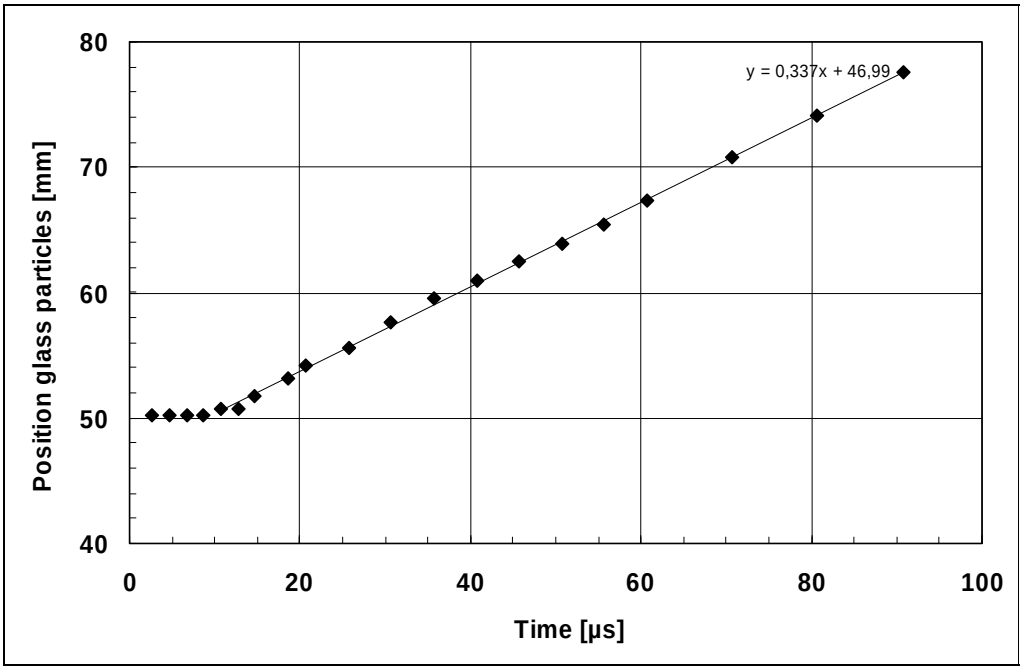

Figure 13. Path-time history of glass particles at the rear side of the 100- × 50-mm Starphire specimen, test no. 15680.

With an air gap of 1.3 mm and a particle velocity of ≅340 m/s, the impact of the glass particles on the edge of the second glass layer could be expected about 3.7 µs after particles separated from the rear edge of the first glass plate.

In test no. 16589 (1.3-mm air gap, crossed polarizers configuration), the first stress wave front was observed in the second glass plate, with a delay of about 3 µs compared to undisturbed wave propagation in a monolithic target. Figure 14 shows a photograph of the target setup (left) and a shadowgraph of the target before the impact test. A selection of eight high-speed photographs in crossed polarizers arrangement is presented in figure 15. The complete set of high-speed photographs is shown in figure A-7 of the appendix. The corresponding path-time histories of wave propagation and fracture propagation in the second glass plate are plotted in figure 16.

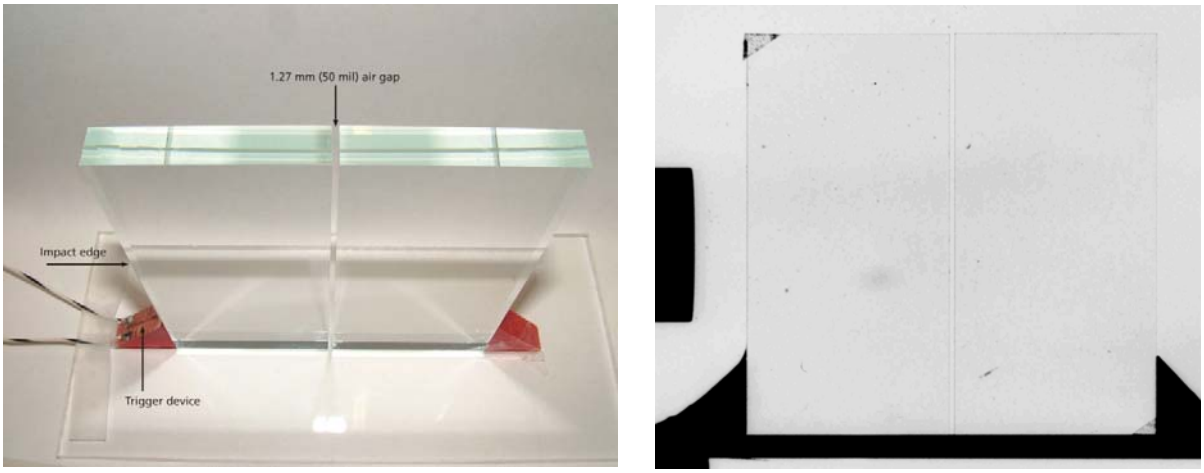

Figure 14. Photograph of target setup (left) and shadowgraph of target (right) before impact, test no. 16589.

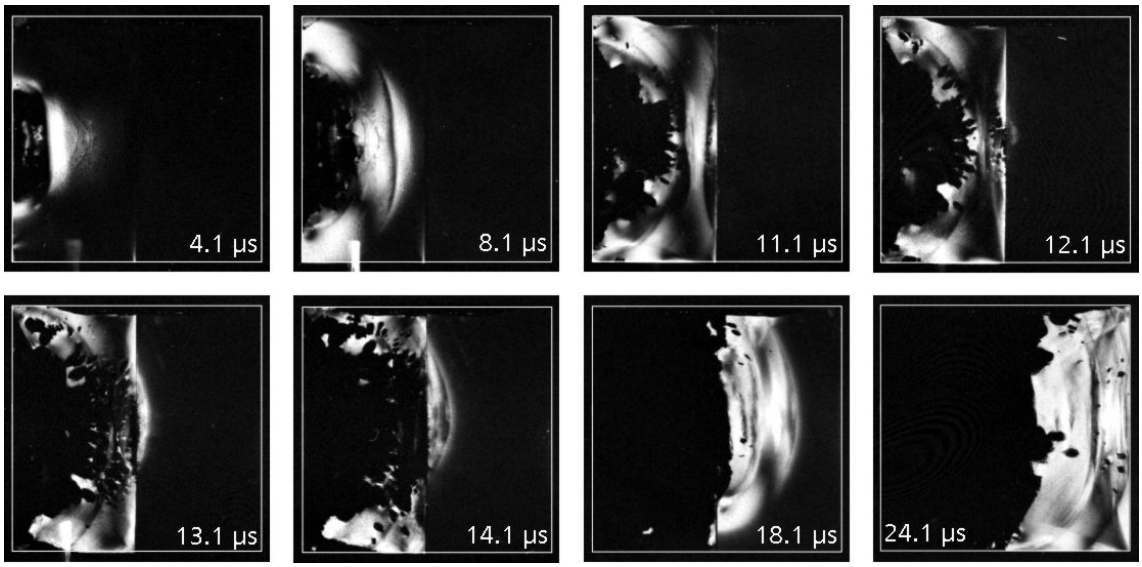

Figure 15. Selection of eight high-speed photographs from test with 1.3-mm air gap between two 100- × 50-mm Starphire glass plates, cylindrical projectile, impact velocity 392 m/s, crossed polarizers, test no. 16589.

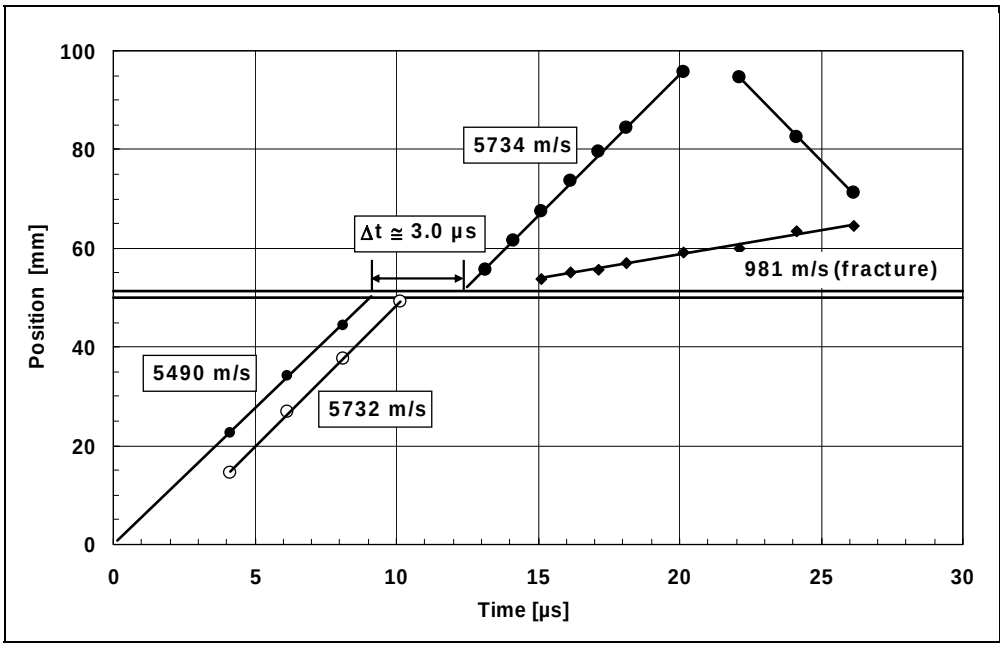

Figure 16. Path-time history of wave and damage propagation in two-layer Starphire target with 1.3-mm air gap, test no. 15689.

It can be recognized from the photographs in figure 15 that at about 12 µs, a stress wave has been initiated in the middle of the front edge of the second glass plate. The evolution of this wave, followed by a damage front and crack centers, can be observed in figure 17.

Another test with a nominal air gap width of 1.3 mm was conducted in a shadowgraph arrangement. Due to inaccurate setup of the specimen, the width of the air gap was significantly smaller. This can be recognized from the selection of eight high-speed photographs in figure 17, where the two glass plates are hardly distinguishable. The complete set of high-speed photographs is presented in figure A-8 of the appendix.

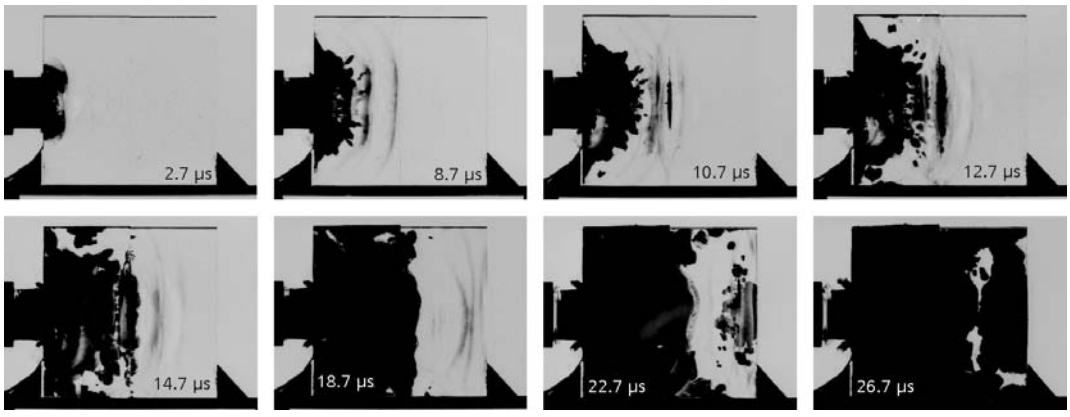

Figure 17. Selection of eight high-speed photographs from test with very small air gap between two 100- × 50-mm Starphire glass plates, cylindrical projectile, impact velocity 387 m/s, crossed polarizers, test no. 16581.

5. Laminated Targets With Strengthened Interlayer

In a previous series of tests,[4] the influence of a layer of chemically strengthened glass on top of a Starphire specimen on damage formation was examined. A comparison of the photographs from the test with a front layer of strengthened glass to those with the unstrengthened front layer revealed no significant differences in the evolution of damage in the case of a cylindrical projectile. The fact that crack formation also occurred in the strengthened layer very shortly after impact could be explained with the high-impact stress levels, which probably exceeded the compressive stresses introduced by the strengthening process.

Therefore, it was decided to examine the effect of a strengthened intermediate layer in a new series of EOI tests. In this case, the stress waves are already attenuated by the first glass layer until they arrive at the strengthened layer. The dimensions of the strengthened interlayer were the same as in the previous set of tests—7.65 × 9.5 × 100 mm. The total dimensions of the specimens were 100 × 100 × 9.5 mm, and the thickness of the bonding layers was 1.27 mm (50 mil). Figure 18 shows a schematic and photograph of a typical specimen. Three types of interlayer were studied: (1) Ion Armor* chemically strengthened glass and unstrengthened glass of the same type as the reference, (2) Corning glass ceramic, and (3) a glass ceramic manufactured by Schott. The test parameters are listed in table 1.

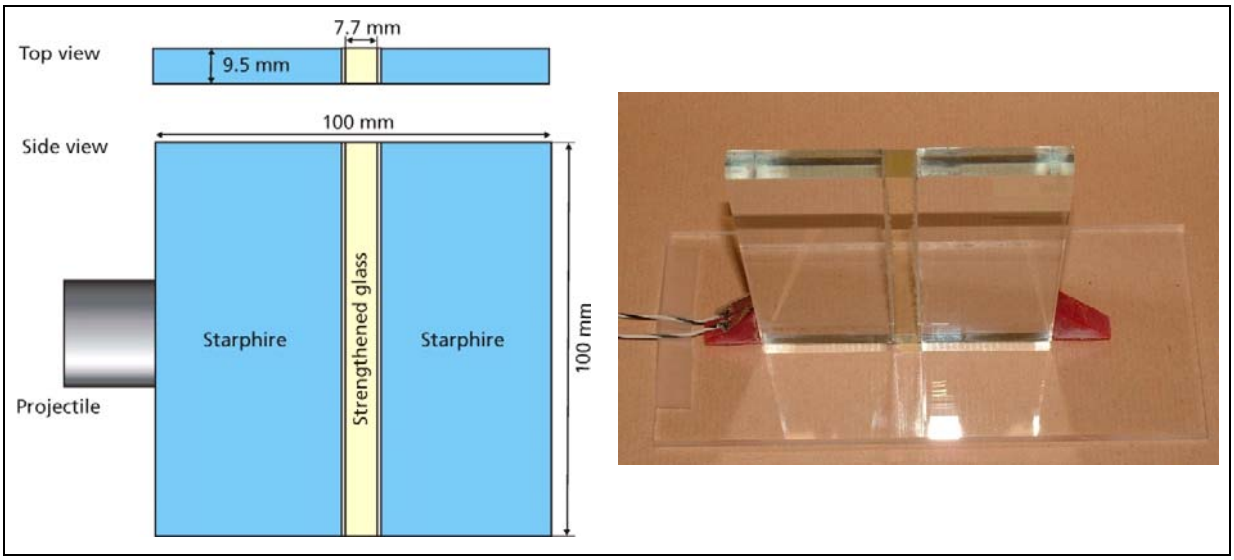

Figure 18. Schematic and photograph of target with strengthened interlayer.

*Ion Armor is a registered trademark of Saxon Glass Technologies, Alfred, NY.

Table 1. Test matrix for samples with strengthened interlayer.

Test No.	Interlayer	V_P (m/s)	Optical Setup	Time Settings (All Tests)			
16582	Ion Armor, strengthened	390	Shadowgraph	2	4	6	8
16583	Ion Armor, unstrengthened	384	Shadowgraph	9	10	11	12
16584	Corning glass ceramic	389	Shadowgraph	13	14	15	16
16585	Corning glass ceramic	385	Crossed polarizers	18	20	22	24
16587	Schott glass ceramics	391	Shadowgraph	28	32	36	40

A comparison of the damage evolution in targets with strengthened and unstrengthened Ion Armor interlayer is presented in figure 19, which shows eight high-speed photographs for each test. The complete sets of high-speed photographs are shown in figures A-9 and A-10 of the appendix.

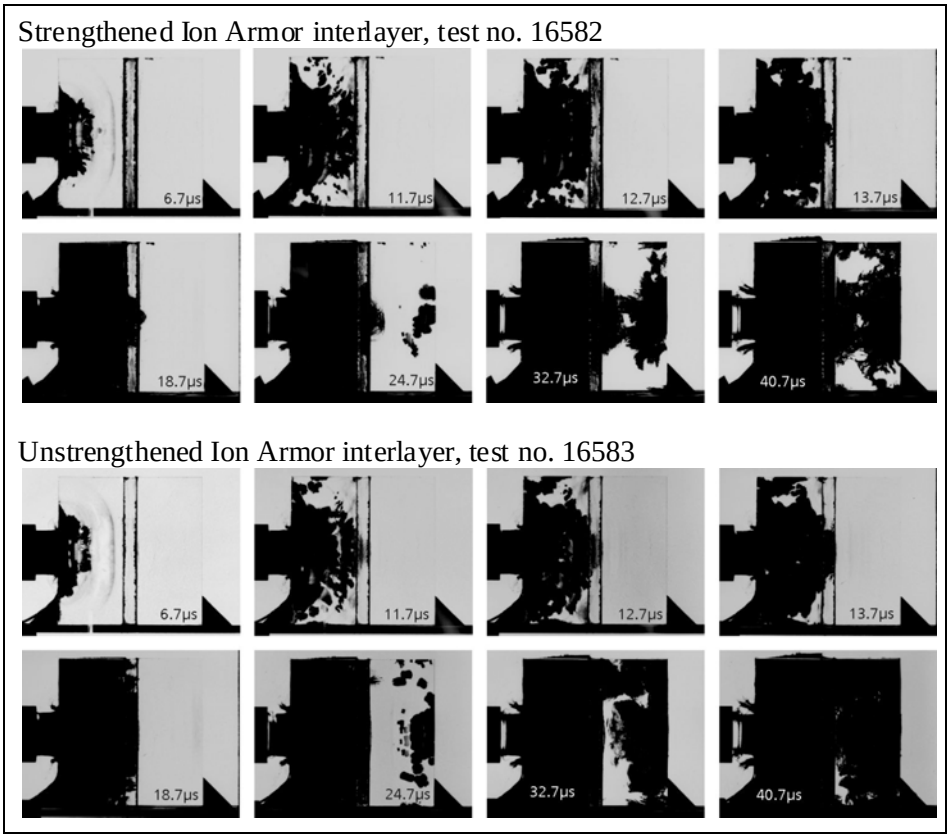

Figure 19. Selection of eight high-speed photographs from tests with strengthened Ion Armor interlayer (top) and unstrengthened Ion Armor interlayer (bottom).

The high-speed photographs in figure 19 reveal that damage evolution in the strengthened interlayer is significantly slower compared to the unstrengthened interlayer. This is confirmed by the quantitative analysis of the fraction of damaged area. The damage evolution curves for the intermediate glass layers are depicted in figure 20. The unstrengthened glass layer

was completely damaged (no light transmission), whereas, after 25 μs, the strengthened Ion Armor exhibited 83% of damaged area at the end of the observation time interval (41 μs).

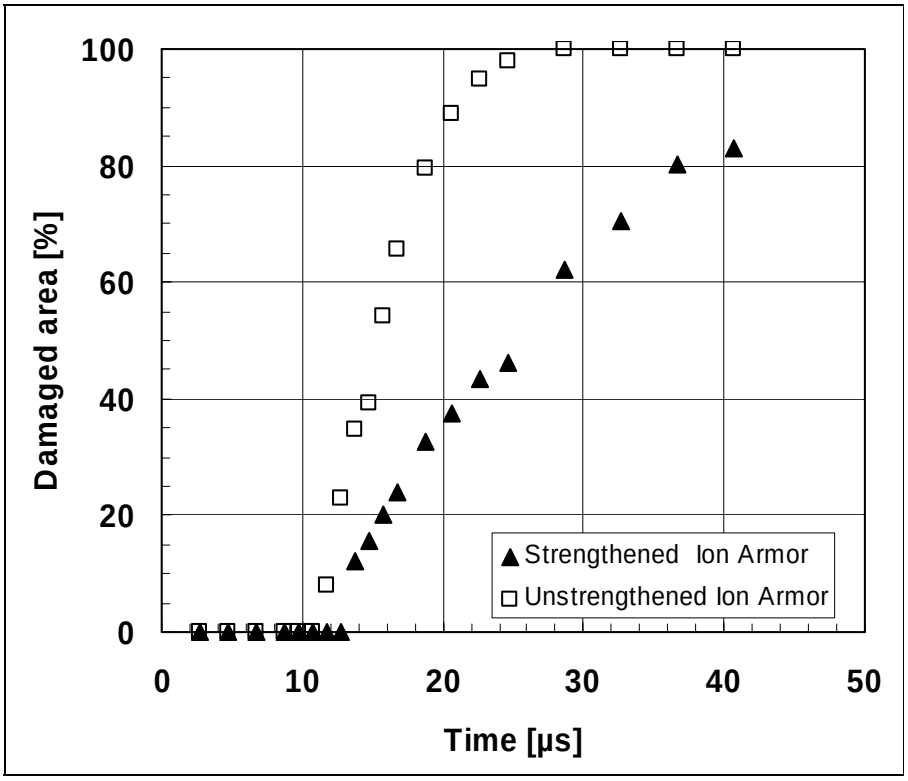

Figure 20. Damage evolution in intermediate Ion Armor glass layers (strengthened and unstrengthened).

Damage in the second Starphire glass plate was mainly generated after the reflection of the stress waves at the rear edge of the specimens. In test no. 15682 (strengthened interlayer), crack propagation from the center of the front edge of the second Starphire plate could also be observed. However, the contribution to the total damage was small, and the overall damaged area observed in the second Starphire plate was bigger in the case of the unstrengthened interlayer. This is illustrated in figure 21, which shows the damage evolution curves for the second Starphire glass plate.

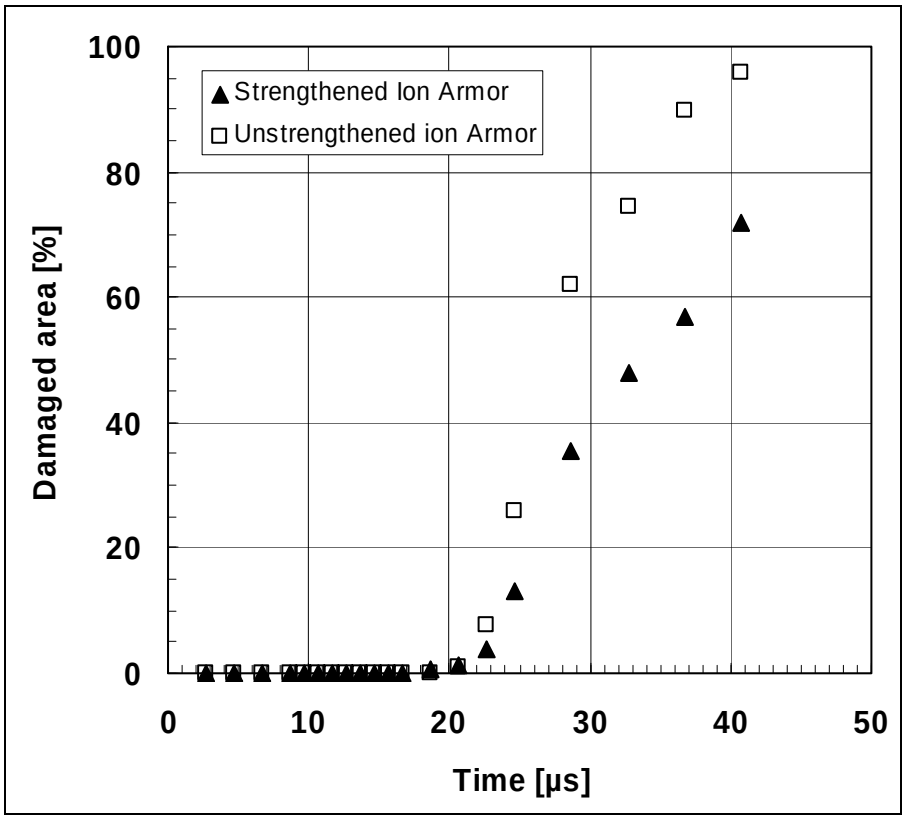

Figure 21. Damage evolution in second Starphire glass plate with intermediate Ion Armor glass layers (strengthened and unstrengthened).

Two tests were conducted with an interlayer of the Corning glass ceramic, one test with the shadowgraph and another test with the crossed polarizers optical setup. The specimen with the Schott glass ceramics interlayer was tested using the shadowgraph configuration. Since the glass ceramic was not polished, it appeared black in the shadowgraphs. A selection of eight high-speed photographs is presented in figure 22. Complete sets of high-speed photographs are presented in figures A-11–A-13 of the appendix.

With the Corning glass ceramic interlayer, damage behavior was observed similar to that in the specimen with the unstrengthened Ion Armor glass interlayer. In contrast, the specimen with the Schott glass ceramic interlayer exhibited a damage-reducing effect similar to the specimen with the strengthened Ion Armor interlayer. The results of the damaged area analysis are presented in figures 23 and 24, which show a comparison of the damage evolution curves in the interlayer and the second Starphire glass plate for the different interlayer materials.

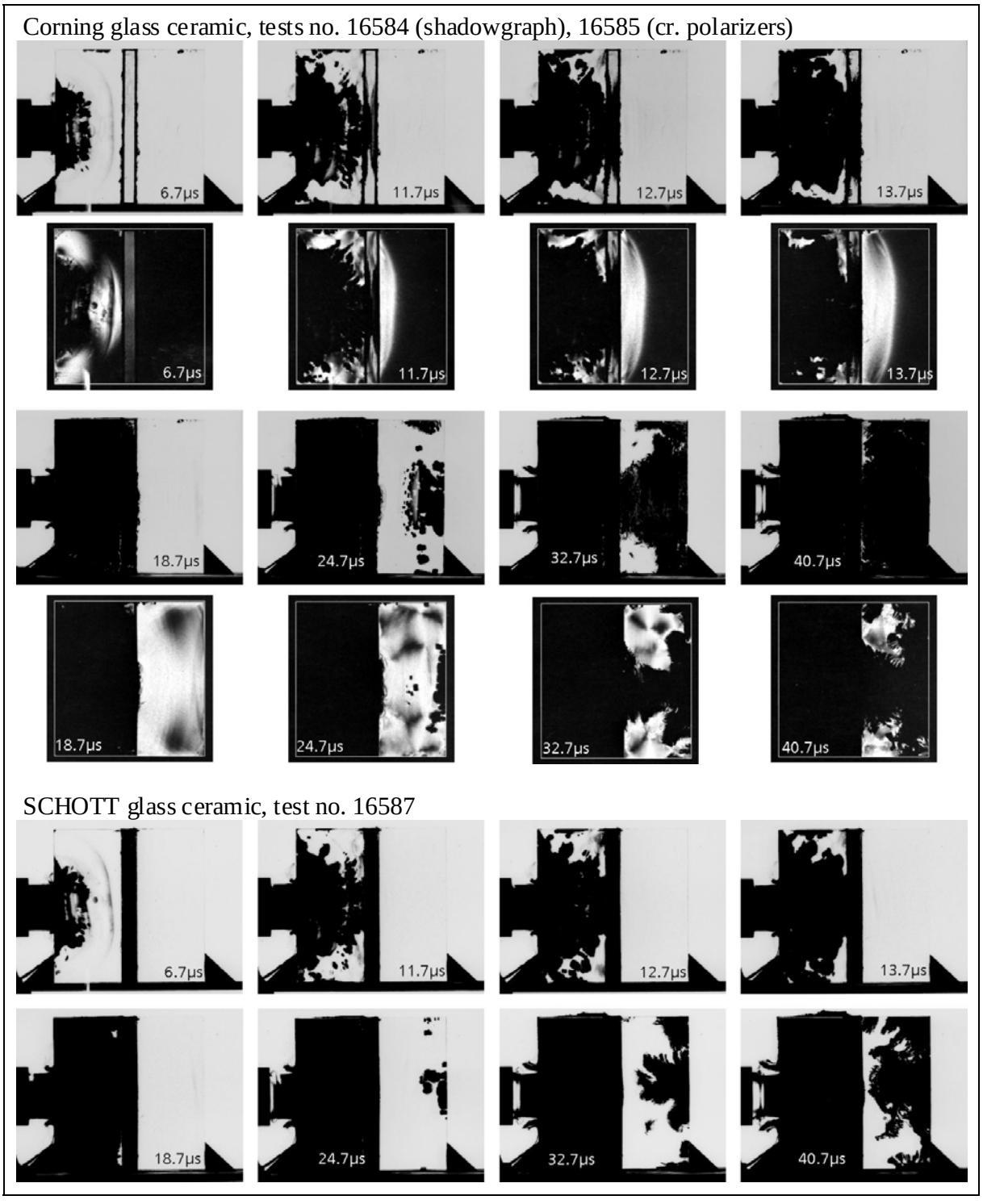

Figure 22. Selection of eight high-speed photographs from tests with glass ceramic interlayer.

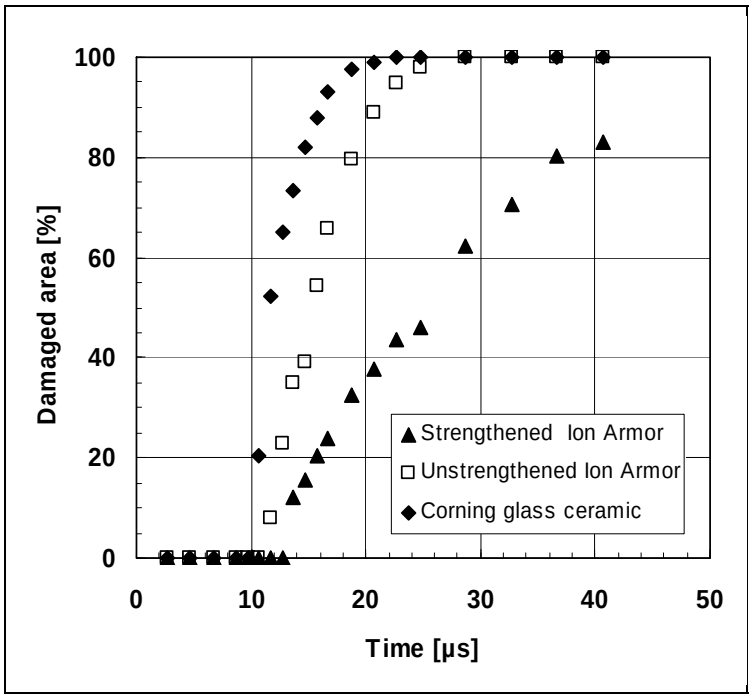

Figure 23. Damage evolution in intermediate glass and glass ceramic layers.

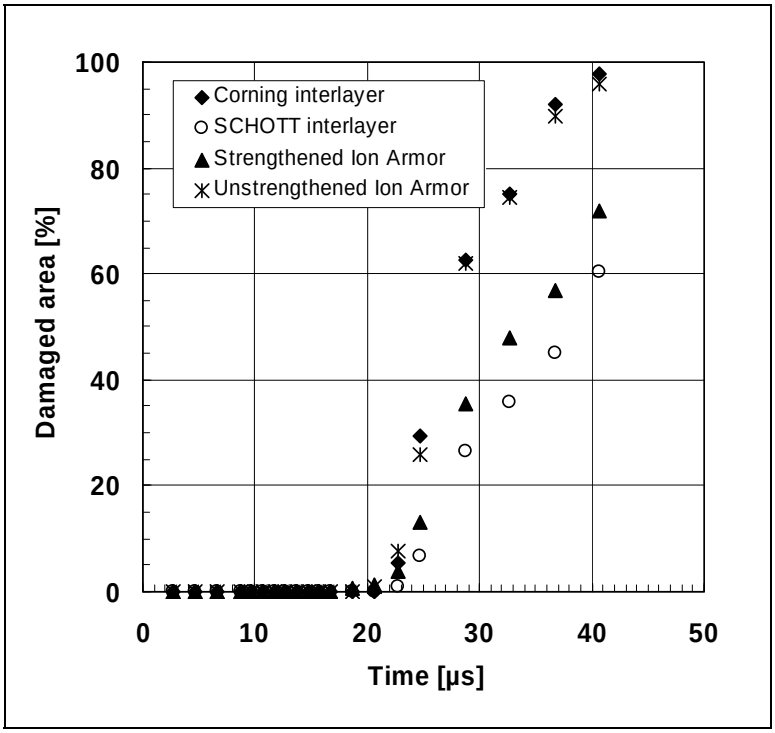

Figure 24. Damage evolution in second Starphire glass plate with intermediate glass and glass ceramic layers.

A comparison of the overall damage development in the specimens with different glass and glass ceramic interlayers is presented in figure 25. Note that the damage evolution curve with the Schott glass ceramic interlayer only consists of the contributions of the two Starphire glass plates since the interlayer was not polished and therefore not transparent. However, the area of the interlayer covers about 7.5% of the total area of the specimen. Thus, the total damaged area fraction can be estimated for the phase of damage evolution in the second Starphire plate by adding about 4%–7% to the displayed values.

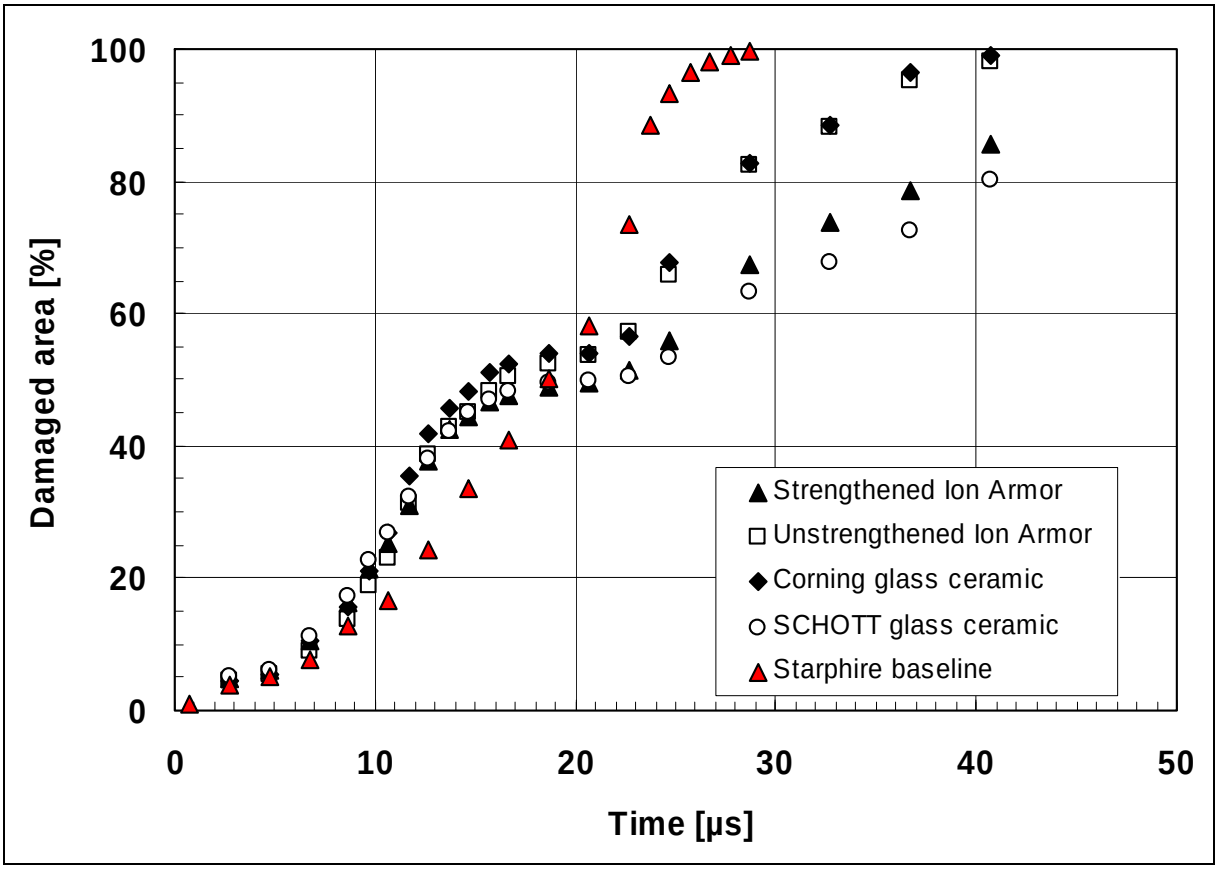

Figure 25. Overall damage evolution in targets with intermediate glass and glass ceramic layers.

6. Two-Layer Laminates at Elevated Temperature

One pair of tests was conducted with a two-layer Starphire laminate with a 1.27-mm-thick (50-mil) bonding layer in a shadowgraph and crossed polarizers optical arrangement. The tests were performed at a specimen temperature of ≈60 °C. To heat up the specimens, a heating box with two copper chambers on the sides and an open bottom was used. The copper chambers were heated up by a flow of 90 °C hot water. The test procedure was as follows:

1. The specimen was aligned in the target box, in front of the gun muzzle.
2. The heating box was put over the specimen, and the specimen was heated up slowly to a temperature above the test temperature.
3. The heating box was removed from the specimen.
4. The impact test was conducted within 2 min after the removal of the heating box to avoid a too-high drop of the specimen temperature.

Figure 26 shows a photograph of an aligned specimen in the target box. Figure 27 illustrates the specimen with the heating box.

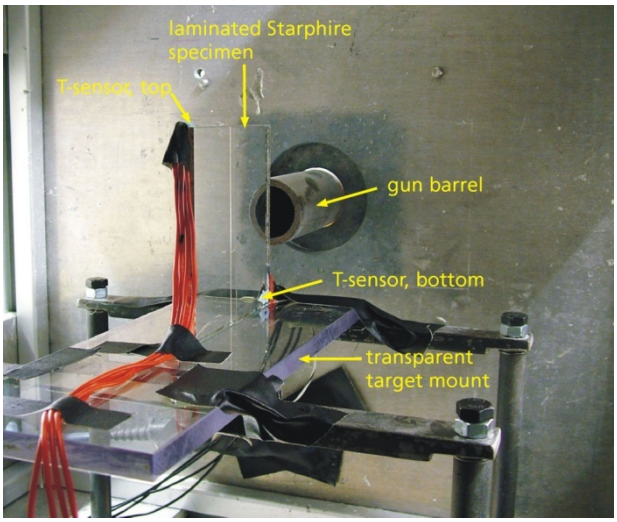

Figure 26. Specimen with temperature sensors aligned in front of the gun muzzle.

Figure 27. Specimen in target chamber with heating box.

The temperature of the specimens was measured by platinum resistance temperature sensors. Two Pt100 platinum chip temperature sensors were glued to the surface of the specimens. Figure 28 shows a photograph of two sensors and their dimensions and a schematic of the sensor construction.

A typical temperature curve after the removal of the heating box is presented in figure 29. The positions of the temperature sensors can be seen from figure 26.

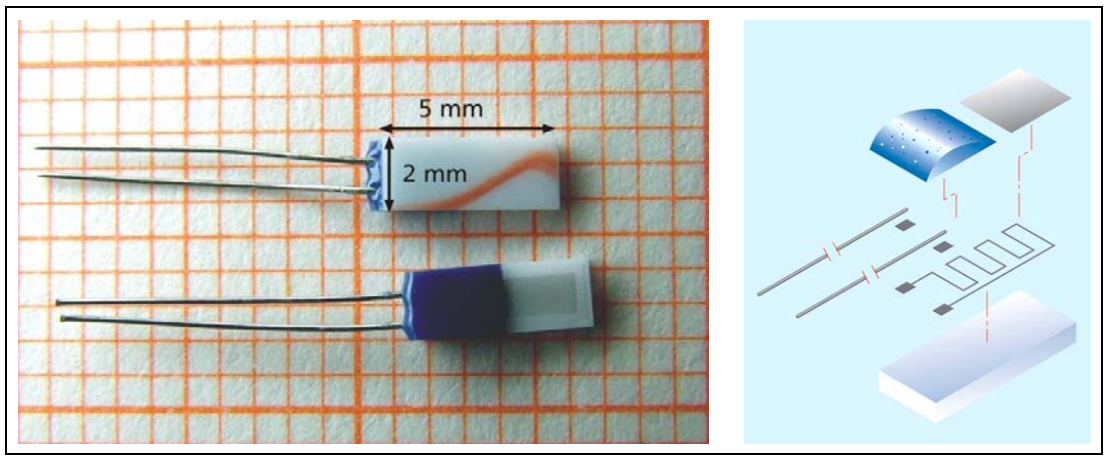

Figure 28. Pt100 temperature sensors.

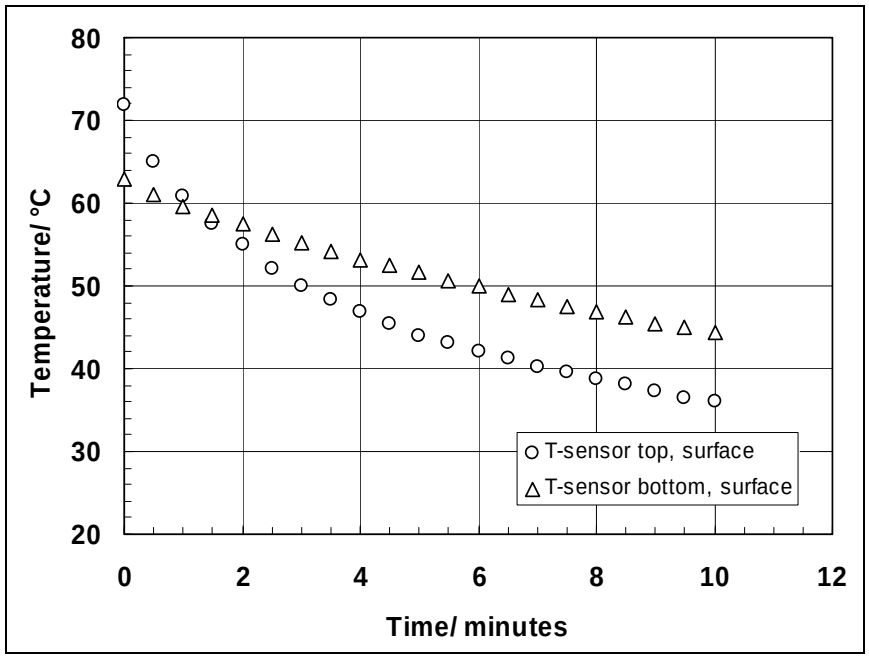

Figure 29. Temperature characteristics of Starphire specimen.

The curves in figure 29 show that the maximum (starting) temperature was higher at the upper edge of the specimen. This is due to the fact that the heating box is open at the bottom, whereas the upper part of the specimen is completely surrounded by the heating box. However, the

temperature drops faster at the upper edge of the specimen when the heating box is removed. The difference between the two curves can be explained by the fact that the lower edge of the specimen is glued to the polycarbonate target mount, which has also been heated up and therefore slows down the temperature drop in the lower part of the specimen during the first minutes. About 1 1/2 min after removal of the heating box, the temperature was nearly equal at both sensor positions.

The EOI tests were performed with temperature sensors only at the surface of the specimens. In order to measure the temperature in the interior of the specimens, especially within the bonding layer, one specimen was instrumented with two additional Pt100 sensors embedded in the bonding layer. Figure 30 shows a schematic and photograph of the specimen and the sensor positions. This specimen was only used for a comparison of the temperature measurements at the surface and in the bonding layer. The results of this measurement are presented in figure 31.

The temperatures measured within the bonding layer after slowly heating the specimen were higher than the temperatures at the surface. Similar to the measurements at the surface, the temperature dropped faster in the upper part of the specimen. However, the difference between the temperature gradients was not as high as with the surface sensors. The curves did not cross during the 10 min of the measurement.

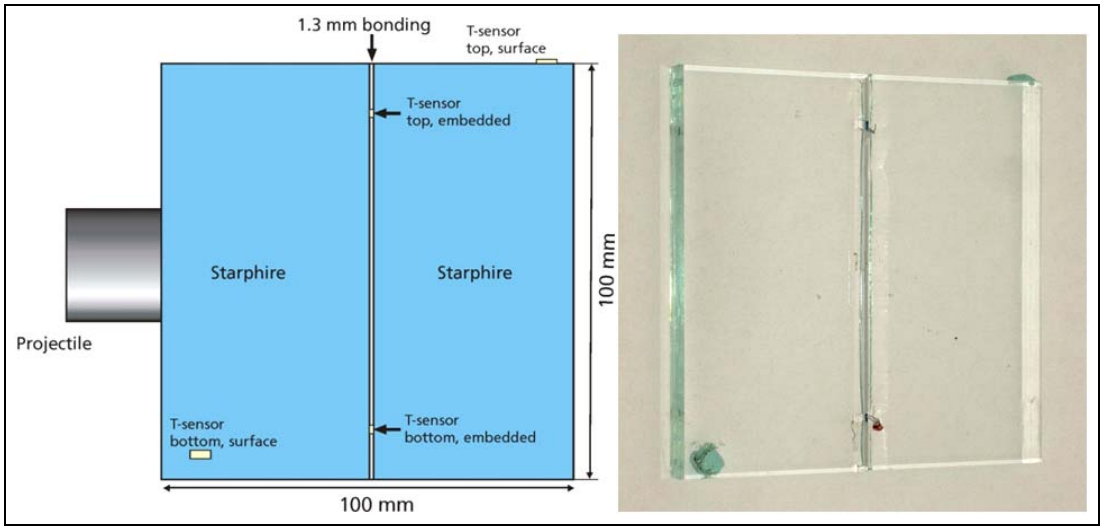

Figure 30. Schematic and photograph of specimen with Pt100 temperature sensors.

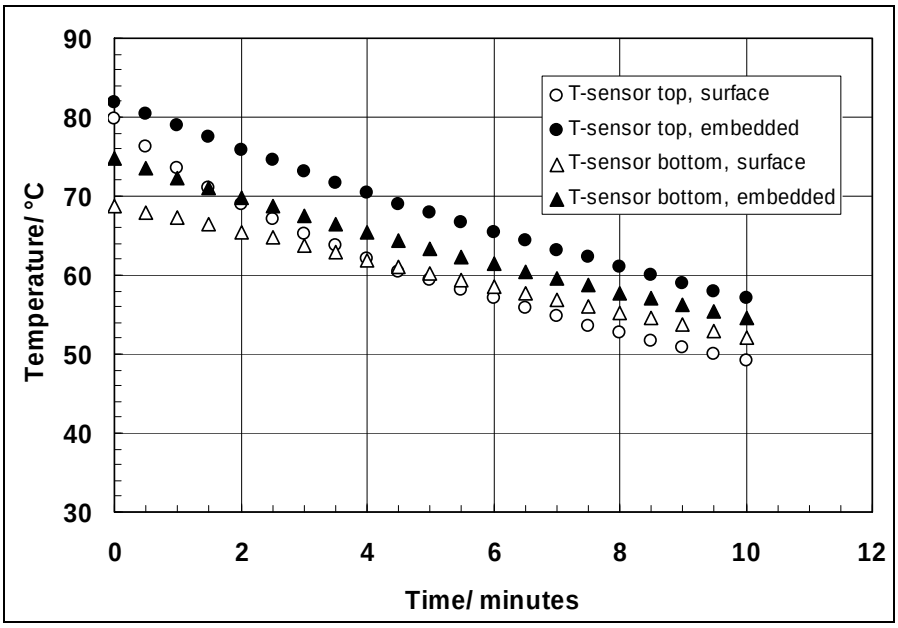

Figure 31. Comparison of temperature characteristics of Starphire specimen with temperature sensors at the surface and embedded in the bonding layer.

The test parameters of the EOI tests at elevated temperature are listed in table 2. The time settings were the same as in the tests with the strengthened interlayer (see table 1). Damage and wave propagation at elevated temperatures is illustrated in figures 32 and 33, which show a selection of eight high-speed photographs from the two tests. The complete sets of high-speed photographs are presented in figures A-14 and A-15 of the appendix.

The high-speed photographs in figures 32 and 33 do not reveal significant differences when compared to the results from tests with equal laminates at room temperatures. This qualitative impression is confirmed by the quantitative damaged area analysis. The damage evolution curve of test no. 16588 is plotted in figure 34, along with the curve from the corresponding test at room temperature (test no. 15299).

The damage evolution curves from both tests are nearly identical. At elevated temperatures, a possible softening of the bonding layer is expected that could lead to a decrease of stiffness and, therefore, an increased bending of the single glass layers in a transparent armor. Compared to the setup used in the EOI tests, the thickness of the glass layers in an armor configuration is much smaller. This could explain why no effect of the elevated temperature was seen in the tests conducted here. The thickness and type of the bonding layer are also expected to play a role in the amount of the effect of elevated temperatures.

Table 2. Test parameters from EOI-tests at elevated temperatures.

Test No.	V_P (m/s)	Optical Setup	Surface Temperature (T) (°C)			
			T_{Max}		T_{Impact}	
			$T_{Sensor\ top}$	$T_{Sensor\ bottom}$	$T_{Sensor\ top}$	$T_{Sensor\ bottom}$
16588	389	Shadowgraph	74.0	57.4	60.0	51.9
16590	398	Crossed polarizers	75.7	63.4	63.4	59.2

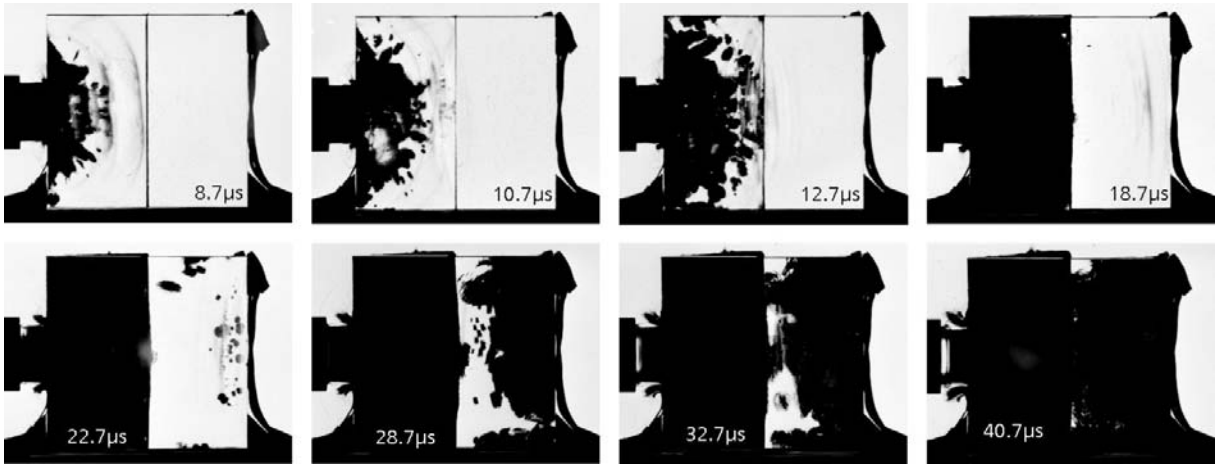

Figure 32. Selection of eight high-speed photographs from test with two-layer Starphire specimen at elevated temperature, impact velocity 389 m/s, test no. 16588.

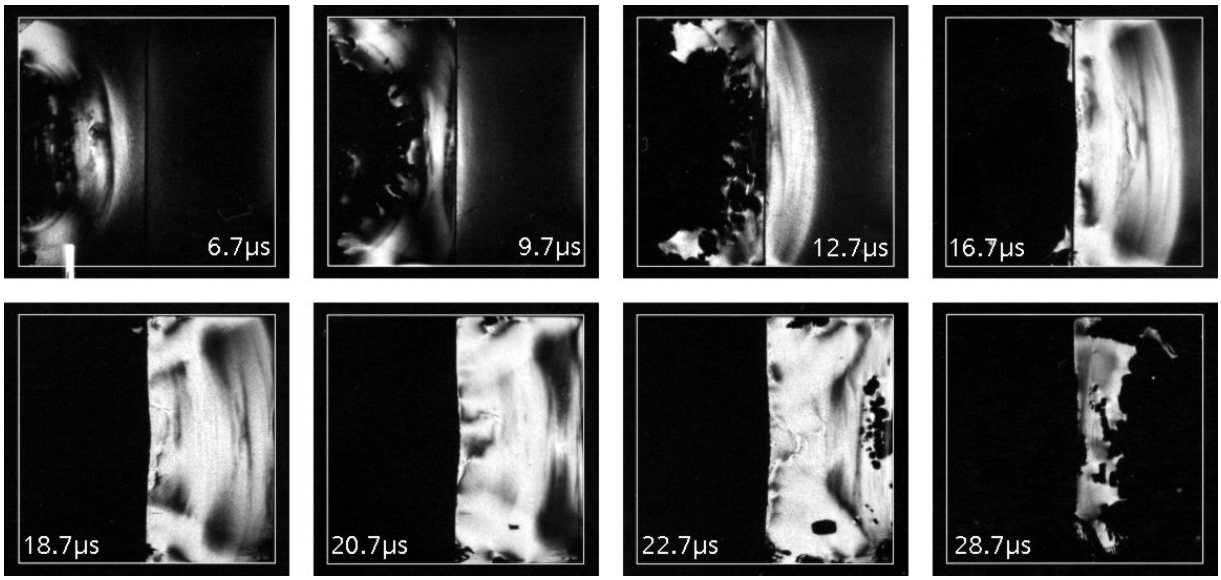

Figure 33. Selection of eight high-speed photographs from test with crossed polarizers configuration, two-layer Starphire specimen at elevated temperature, v_P = 398 m/s, test no. 16590.

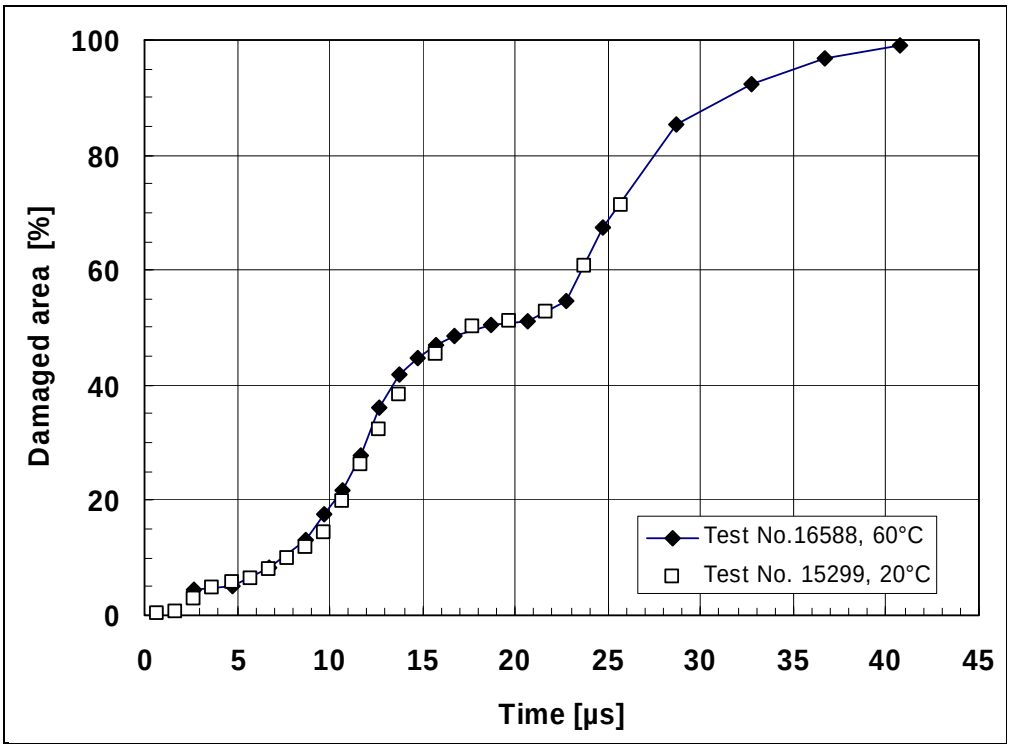

Figure 34. Damage evolution curves from tests with two-layer Starphire laminates at elevated and room temperatures.

7. Conclusions

The focus of this study was on the investigation of the influence of a layer of strengthened glass or glass ceramic in a laminate target and the influence of elevated temperatures on wave and damage propagation.

Baseline tests with different glasses, using cylindrical and spherical projectiles and extended time intervals of observation, showed agreement with damage evolution in previous tests.

In contrast to previous results with Ion Armor front layers, damage evolution was significantly slower when Ion Armor-strengthened glass was used as interlayer. Damage in the second Starphire layer was also reduced in the case of the strengthened Ion Armor interlayer.

Two types of glass ceramic were also tested as interlayer. With a Schott glass ceramic interlayer, a damage-reducing effect similar to the specimen with the strengthened Ion Armor interlayer was observed. With the Corning glass ceramic interlayer, damage behavior was observed similar to that in the specimen with the unstrengthened Ion Armor glass interlayer.

Edge-on Impact tests with two-layer Starphire laminates at temperatures of ≈60 °C did not reveal a different damage behavior compared to tests at room temperature.

INTENTIONALLY LEFT BLANK.

Appendix. High-Speed Photographs

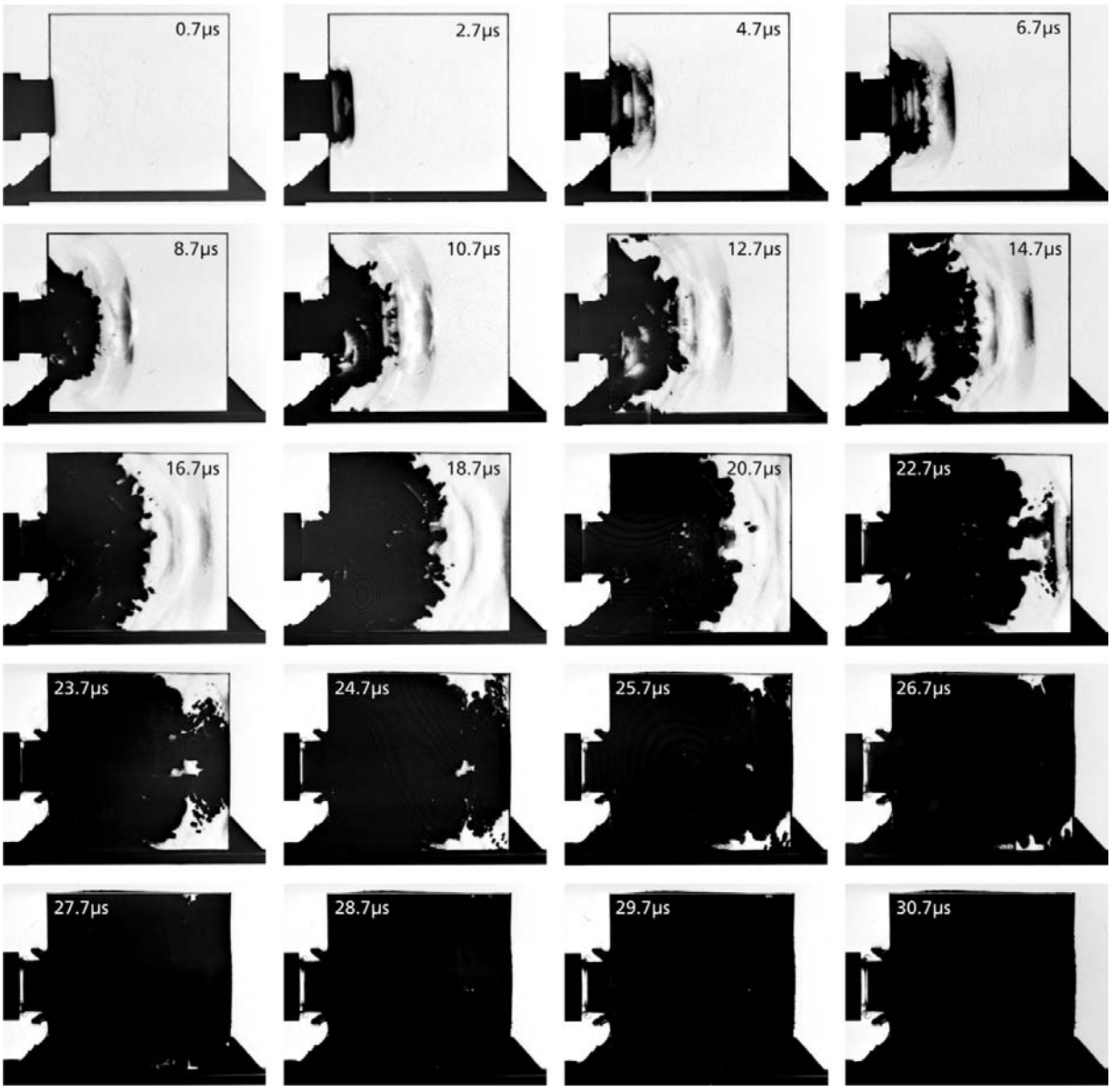

Figure A-1. Complete set of high-speed photographs from baseline test with Borofloat, cylindrical projectile, impact velocity 392 m/s, test no. 16591.

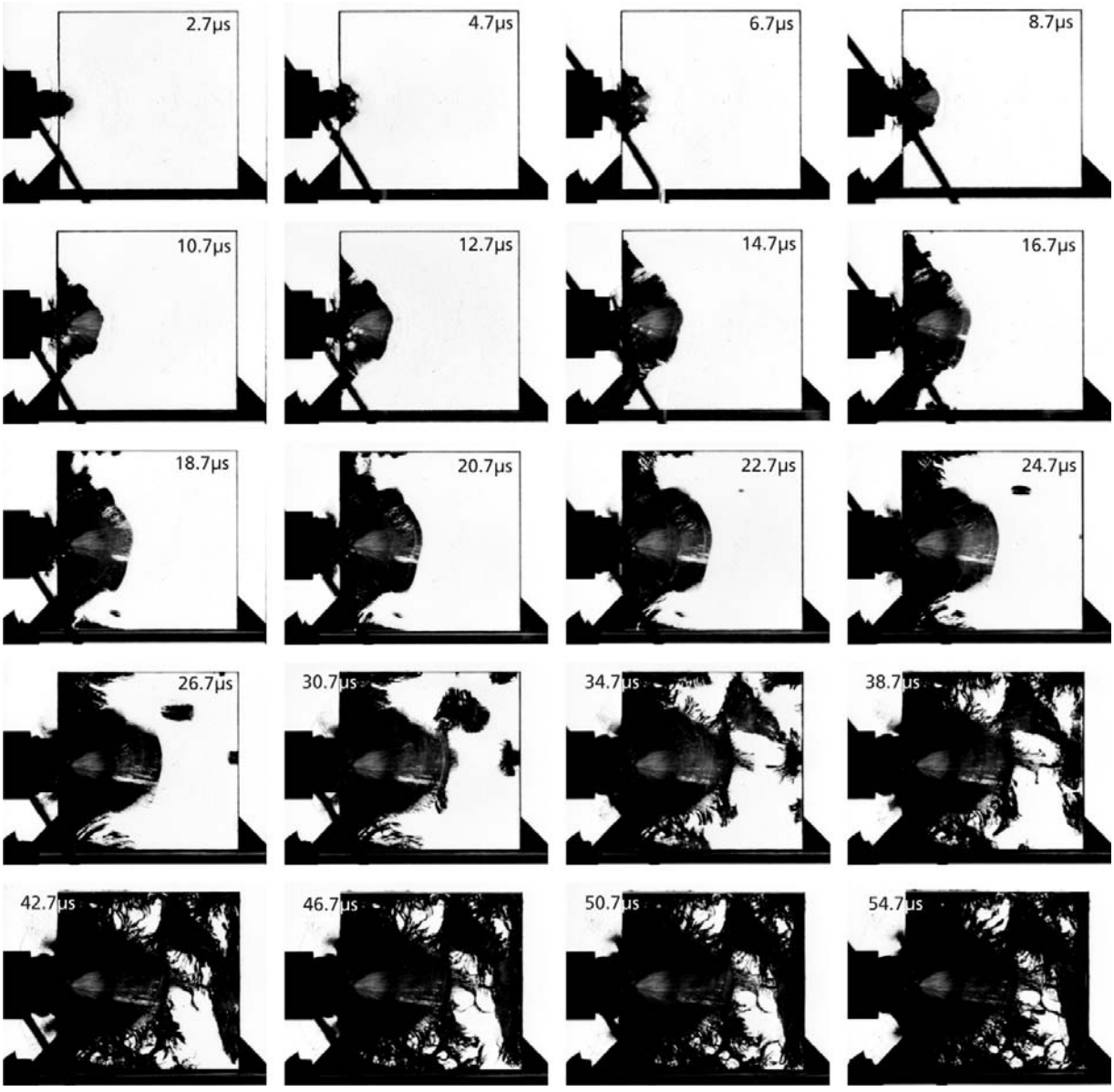

Figure A-2. Complete set of high-speed photographs from baseline test with Borofloat, spherical projectile, impact velocity 435 m/s, test no. 16594.

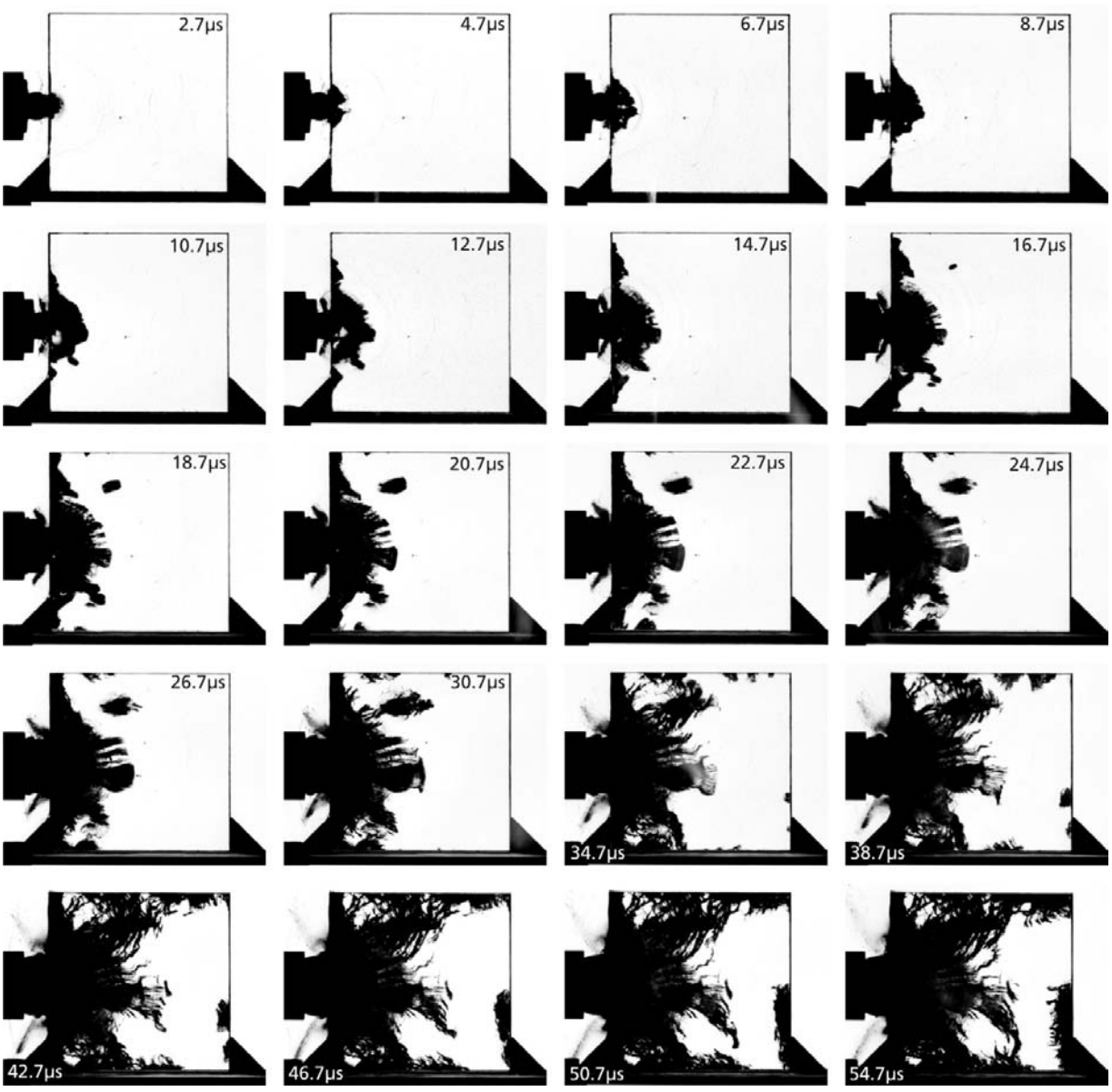

Figure A-3. Complete set of high-speed photographs from baseline test with Starphire, spherical projectile, impact velocity 432 m/s, test no. 16595.

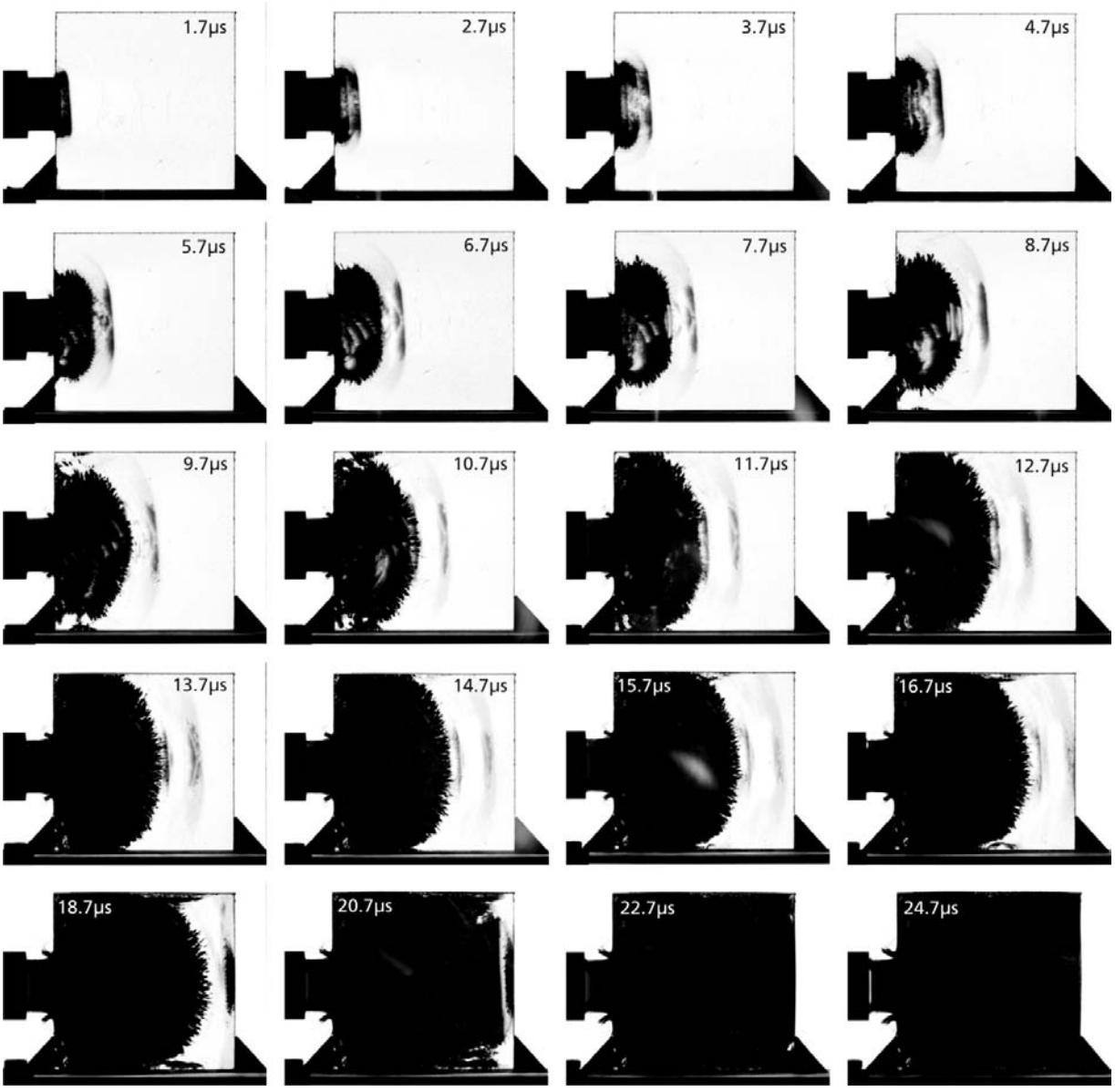

Figure A-4. Complete set of high-speed photographs from baseline test with Corning glass ceramic, cylindrical projectile, impact velocity 388 m/s, test no. 16592.

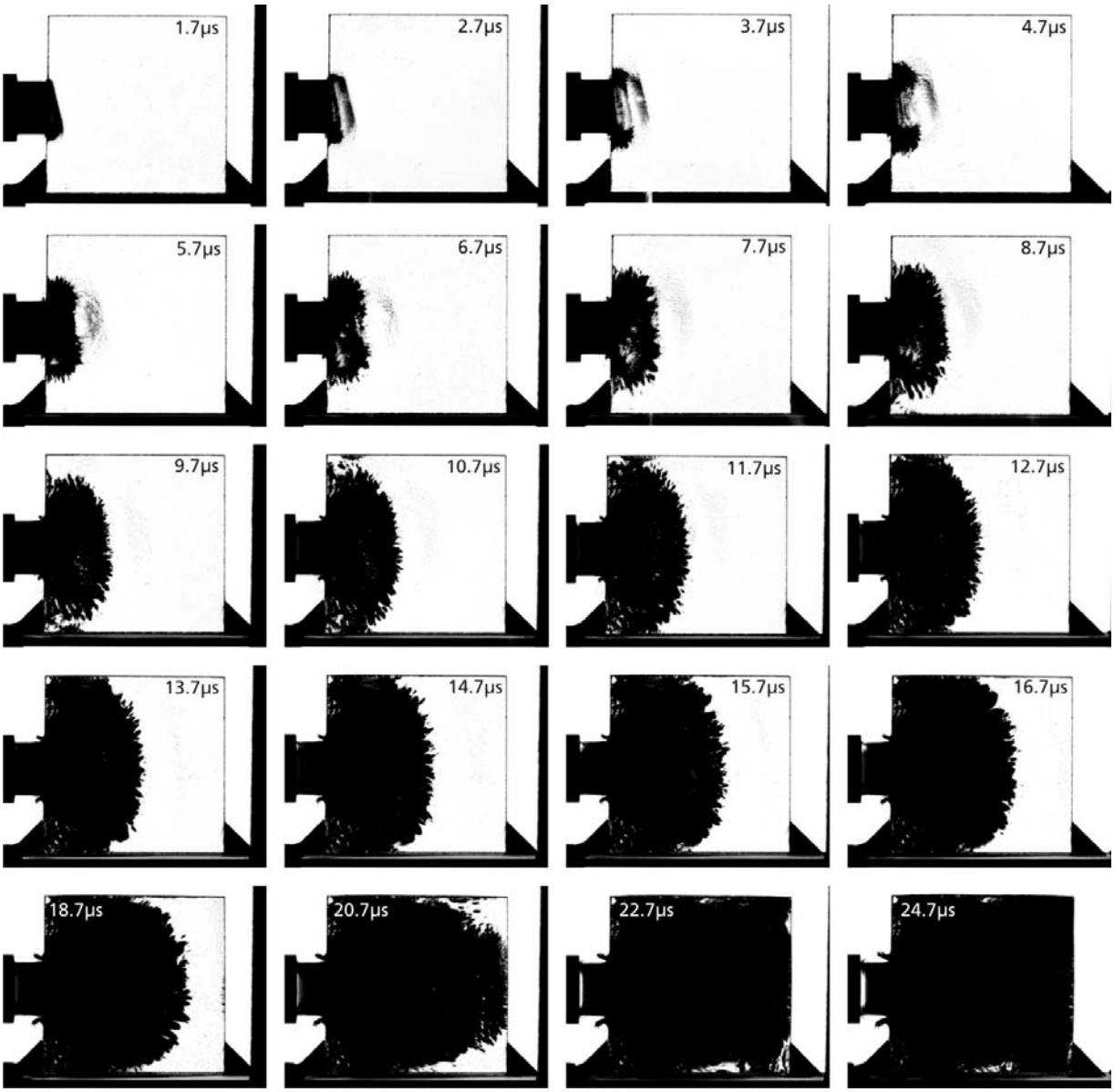

Figure A-5. Complete set of high-speed photographs from baseline test with Schott glass ceramic, cylindrical projectile, impact velocity 393 m/s, test no. 16593.

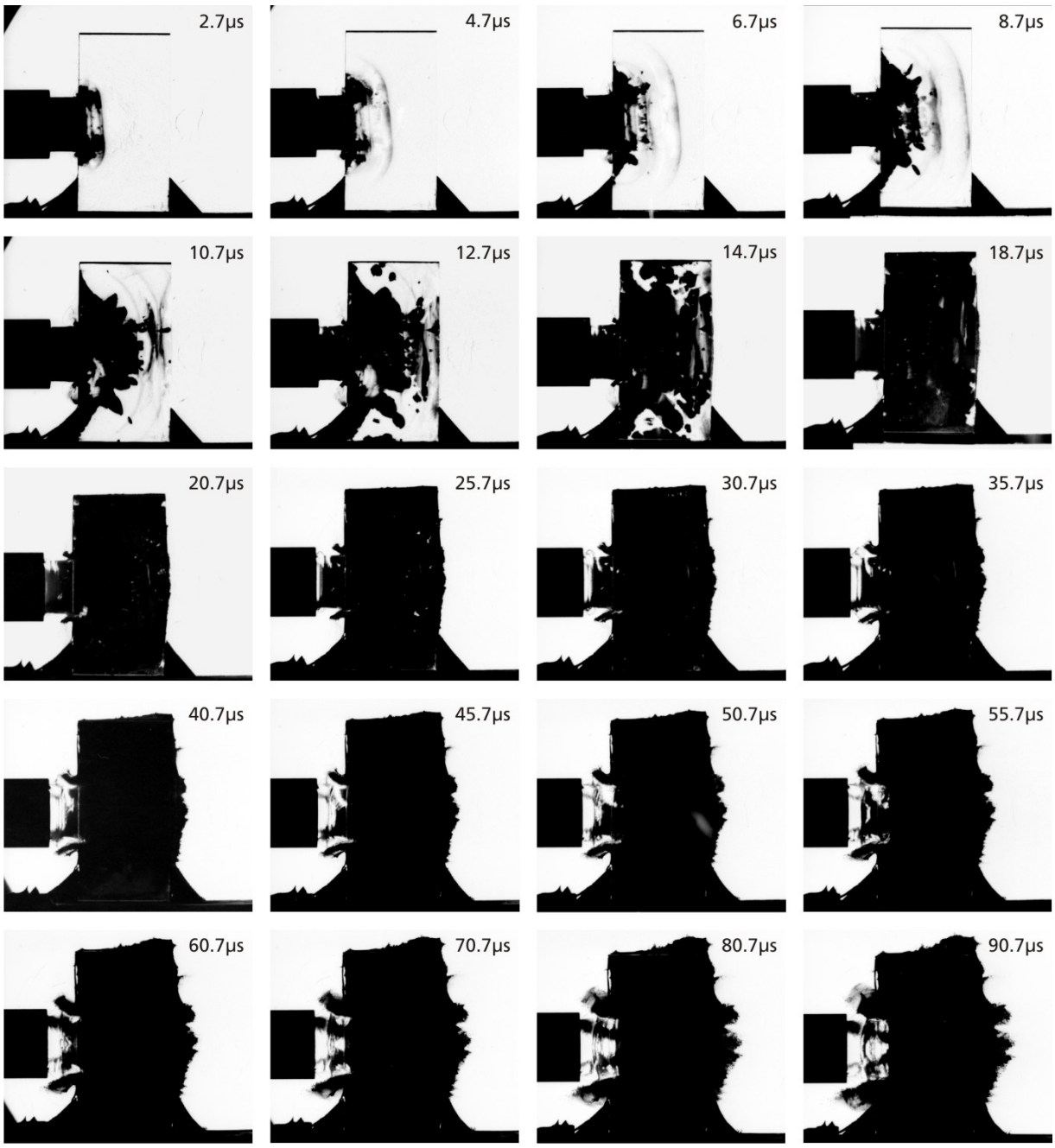

Figure A-6. Complete set of high-speed photographs from test with the 100- × 50-mm Starphire specimen, cylindrical projectile, impact velocity 388 m/s, test no. 16580.

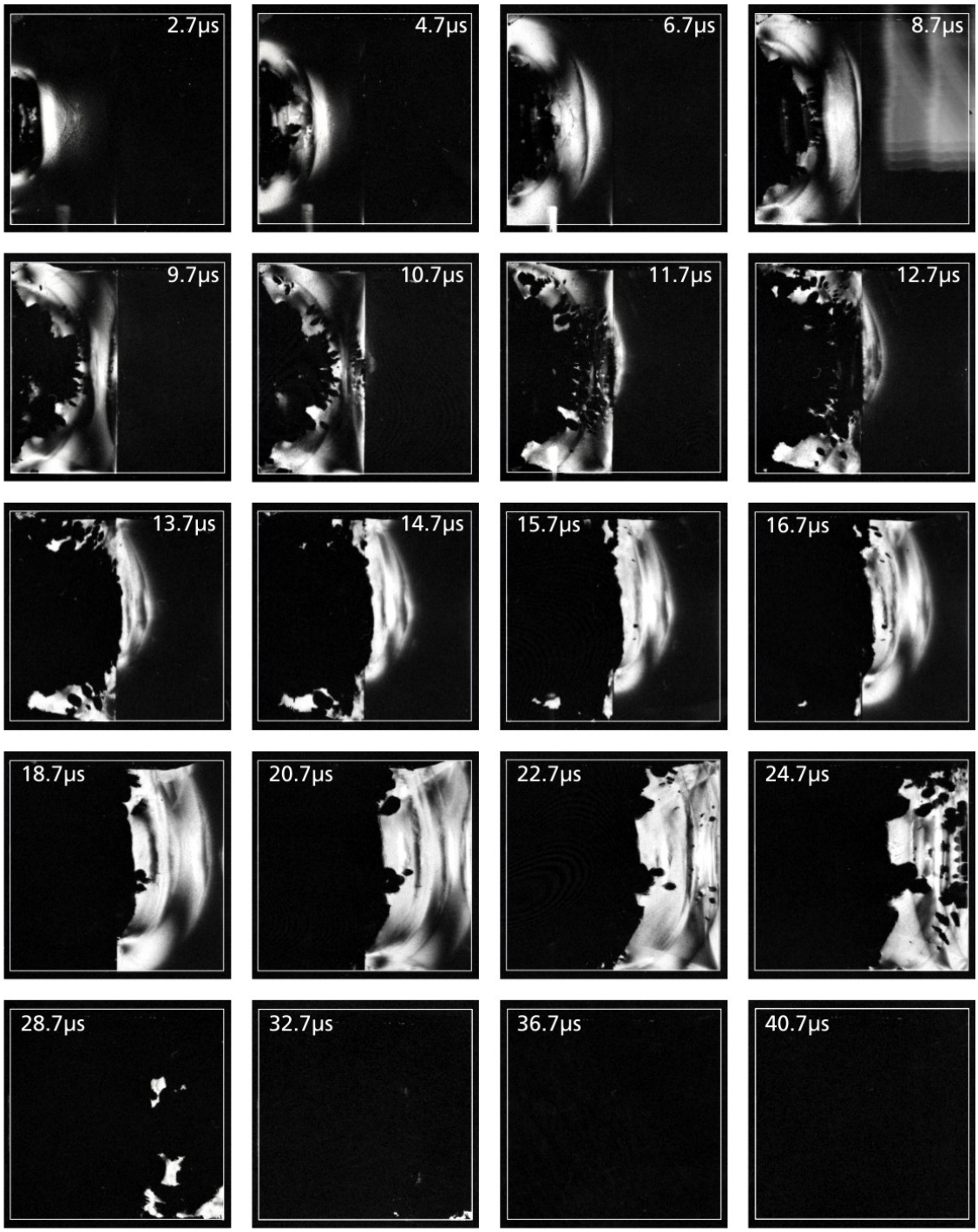

Figure A-7. Complete set of high-speed photographs from test with 1.3-mm air gap between two 100- × 50-mm Starphire glass plates, cylindrical projectile, impact velocity 392 m/s, crossed polarizers, test no. 16589.

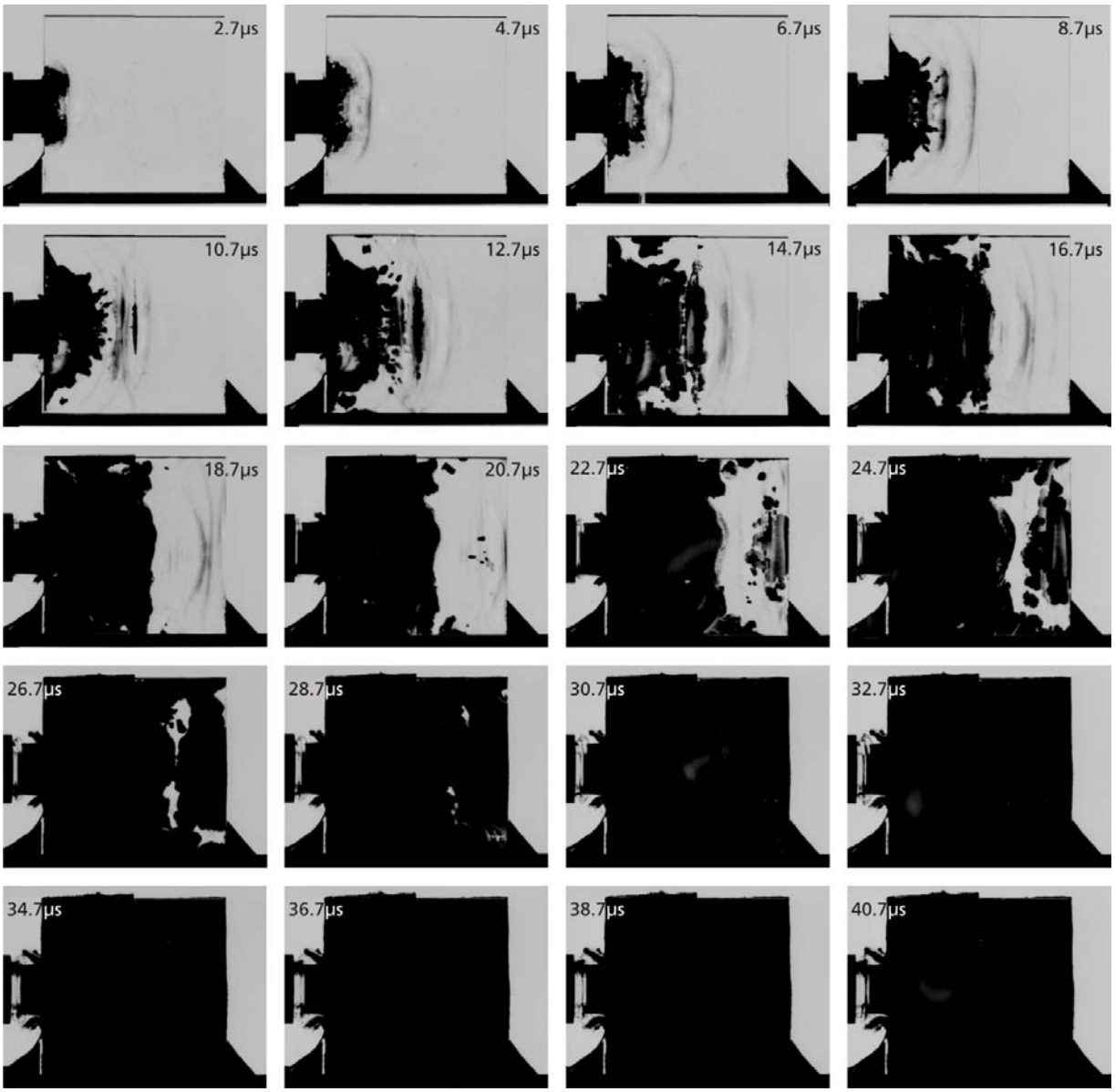

Figure A-8. Complete set of high-speed photographs from test with very small air gap between two 100- × 50-mm Starphire glass plates, cylindrical projectile, impact velocity 387 m/s, test no. 16581.

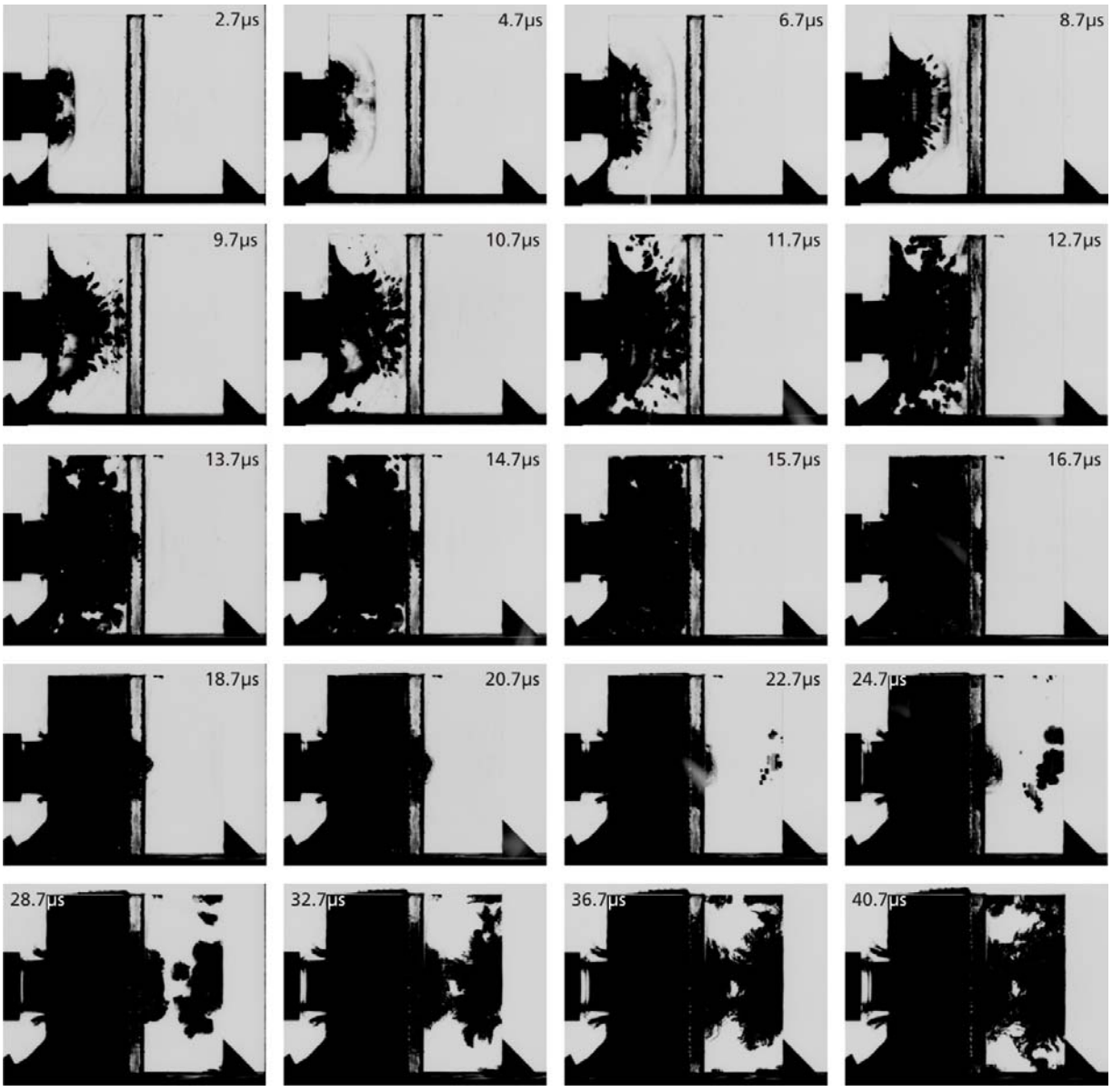

Figure A-9. Complete set of high-speed photographs from test with strengthened Ion Armor interlayer, cylindrical projectile, impact velocity 390 m/s, test no. 16582.

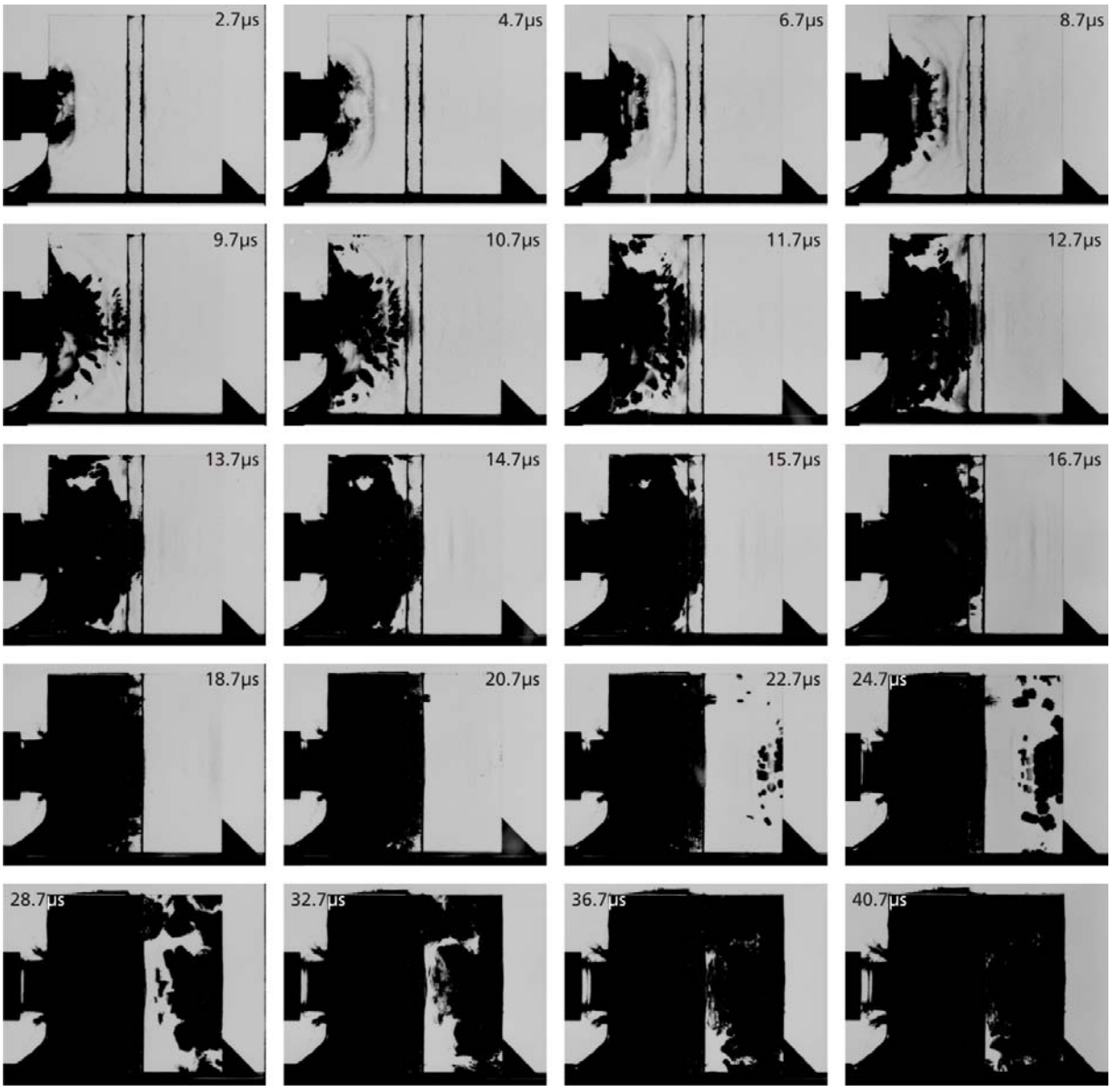

Figure A-10. Complete set of high-speed photographs from test with unstrengthened Ion Armor interlayer, cylindrical projectile, impact velocity 384 m/s, test no. 16583.

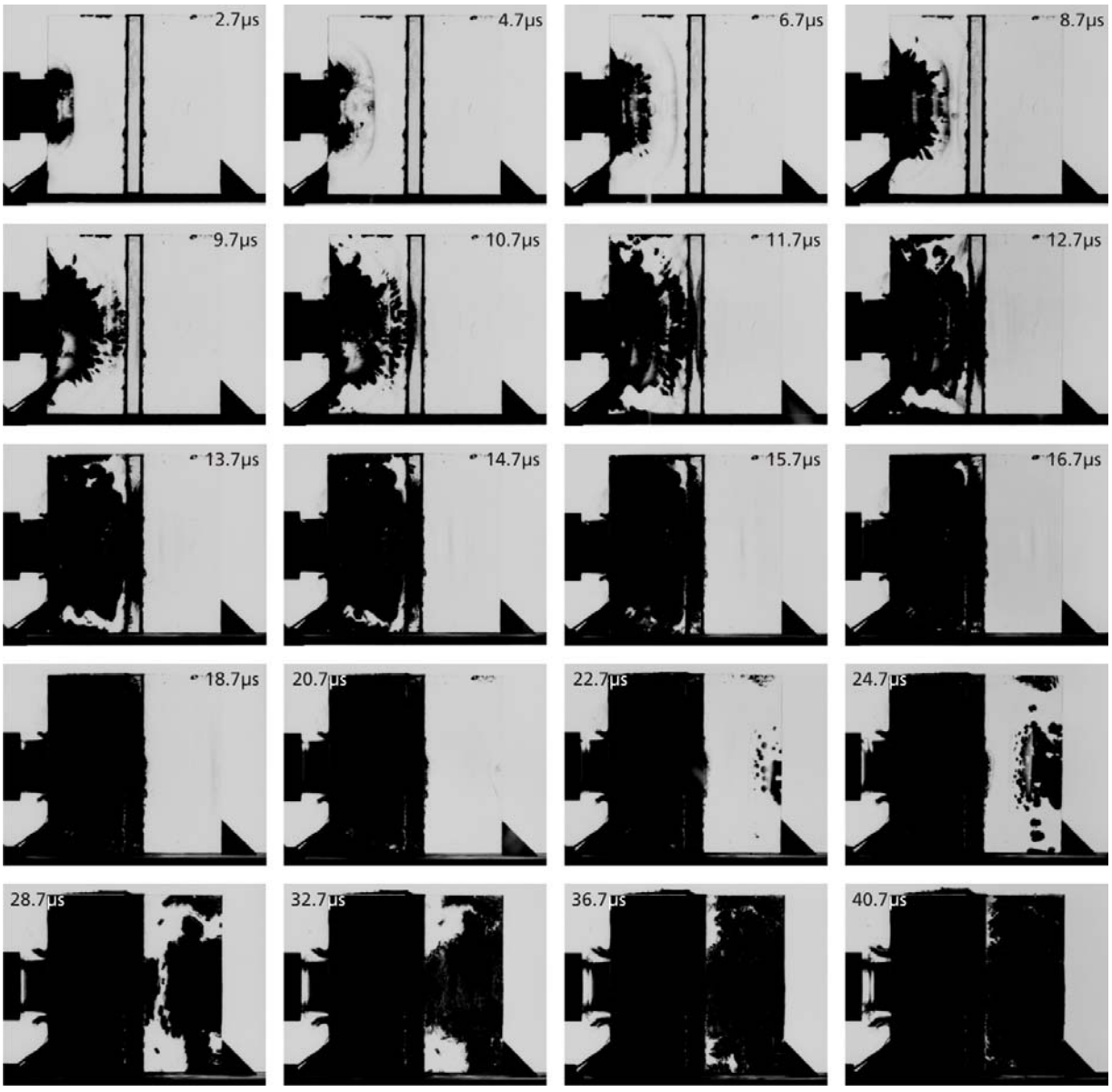

Figure A-11. Complete set of high-speed photographs from test with Corning glass ceramic interlayer, cylindrical projectile, impact velocity 389 m/s, test no. 16584.

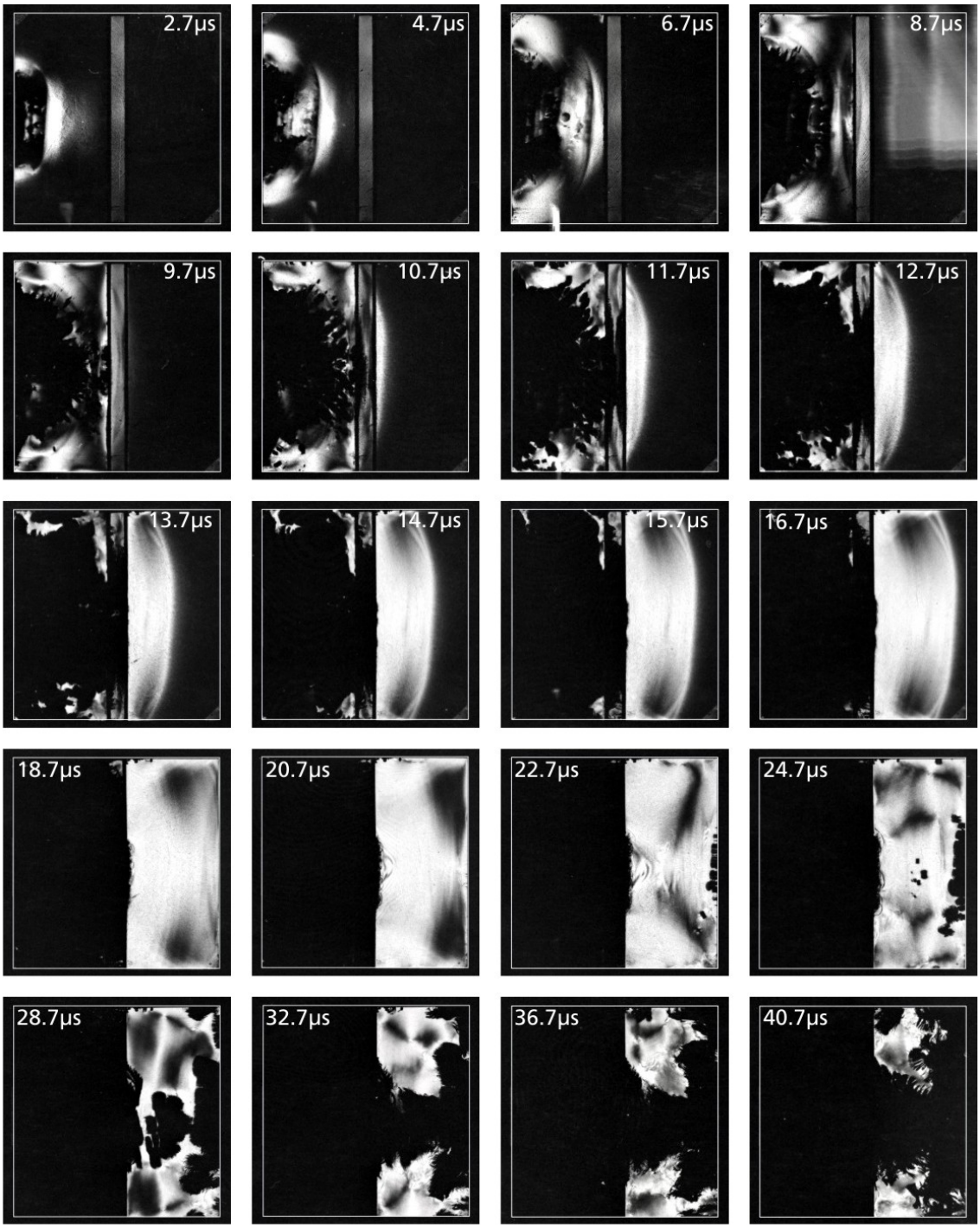

Figure A-12. Complete set of high-speed photographs from test with Corning glass ceramic interlayer, crossed polarizers, cylindrical projectile, impact velocity 385 m/s, test no. 16585.

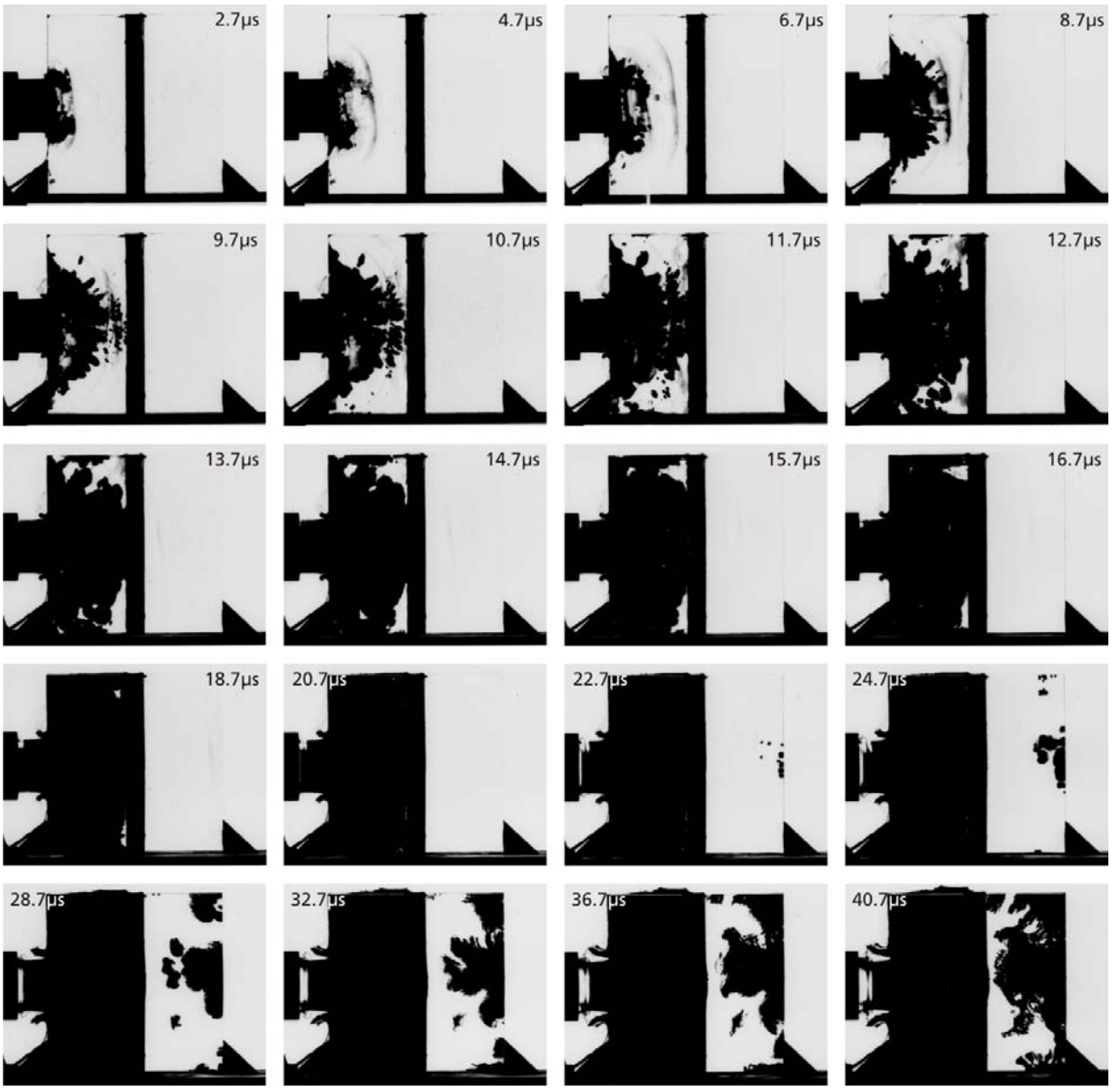

Figure A-13. Complete set of high-speed photographs from test with Schott glass ceramic interlayer, cylindrical projectile, impact velocity 391 m/s, test no. 16587.

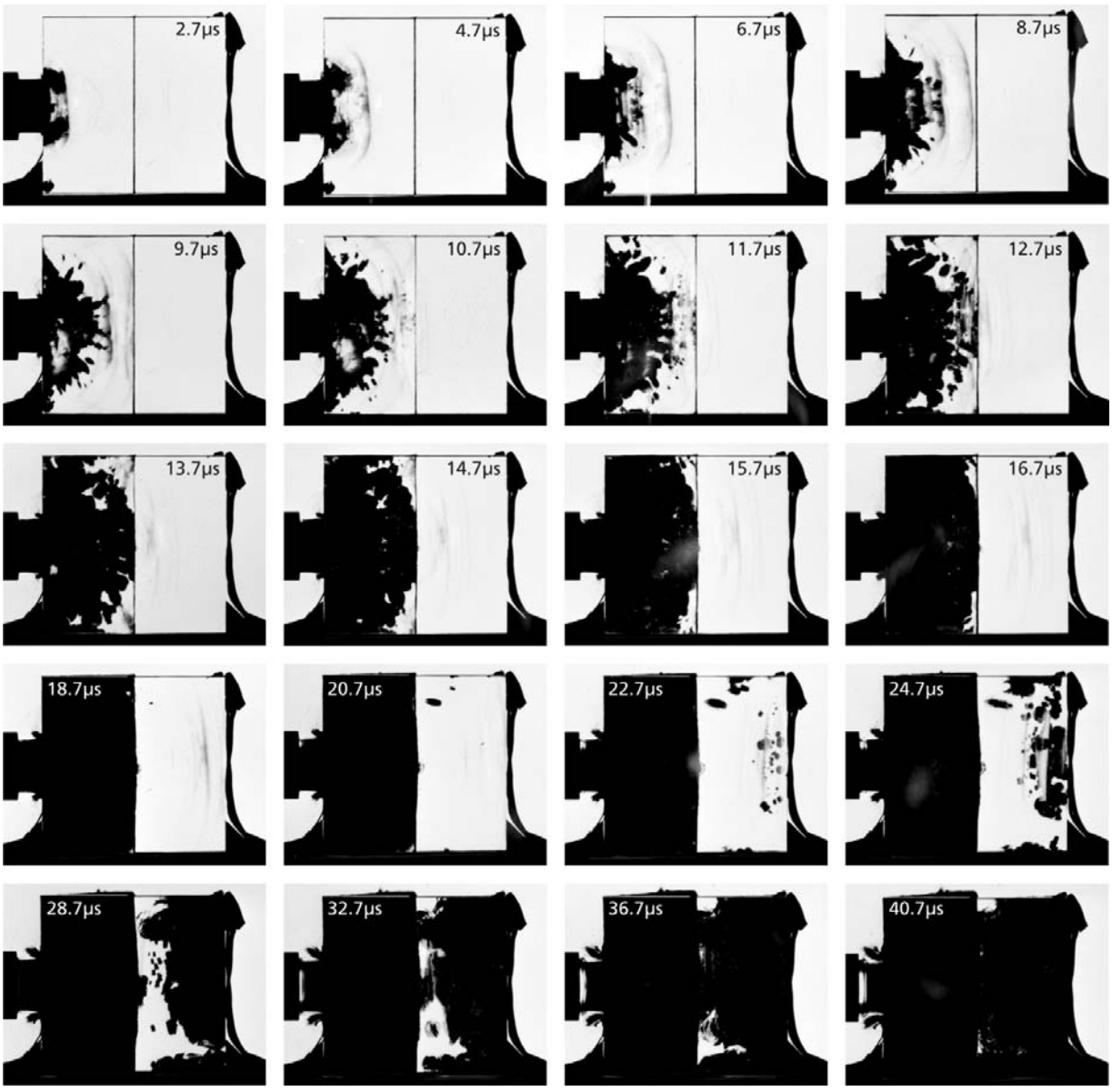

Figure A-14. Complete set of high-speed photographs from test with two-layer Starphire laminate at ≈60 °C, cylindrical projectile, impact velocity 389 m/s, test no. 16588.

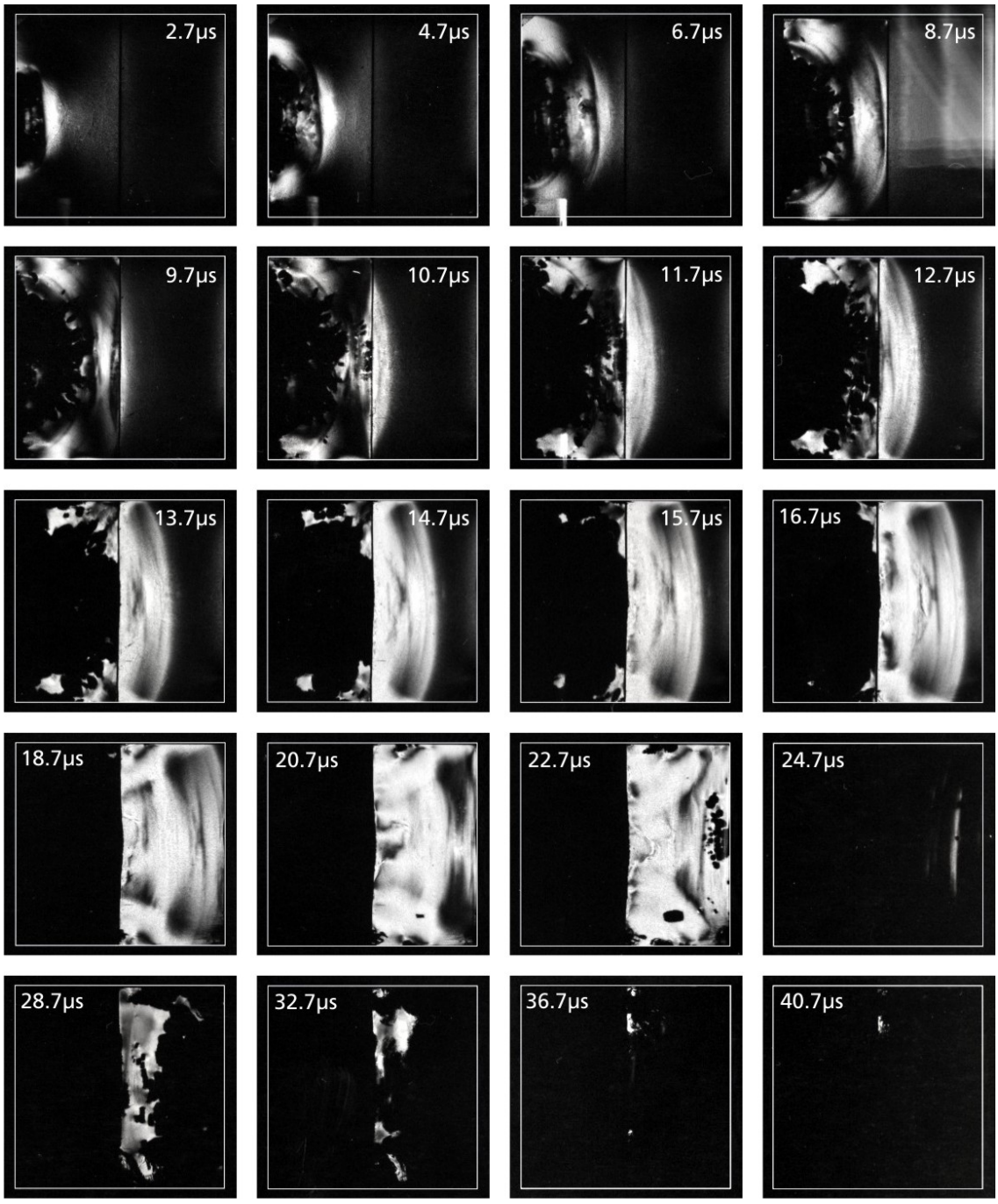

Figure A-15. Complete set of high-speed photographs from test with two-layer Starphire laminate at ≈60 °C, crossed polarizers, cylindrical projectile, impact velocity 398 m/s, test no. 16590.

NO. OF
COPIES ORGANIZATION

1 (PDF only) DEFENSE TECHNICAL INFORMATION CTR
DTIC OCA
8725 JOHN J KINGMAN RD
STE 0944
FORT BELVOIR VA 22060-6218

1 DIRECTOR
US ARMY RESEARCH LAB
IMNE ALC HRR
2800 POWDER MILL RD
ADELPHI MD 20783-1197

1 DIRECTOR
US ARMY RESEARCH LAB
RDRL CIM L
2800 POWDER MILL RD
ADELPHI MD 20783-1197

1 DIRECTOR
US ARMY RESEARCH LAB
RDRL CIM P
2800 POWDER MILL RD
ADELPHI MD 20783-1197

ABERDEEN PROVING GROUND

1 DIR USARL
RDRL CIM G (BLDG 4600)

NO. OF COPIES	ORGANIZATION
1	ODUSD SANDT WS L SLOTER ROSSLYN PLAZA N STE 9030 1777 N KENT ST ARLINGTON VA 22209-2210
1	COMMANDER US ARMY MATERIEL CMND AMXMI INT 9301 CHAPEK RD FT BELVOIR VA 22060-5527
1	PEO GCS SFAE GCS BCT MS 325 M RYZYI 6501 ELEVEN MILE RD WARREN MI 48397-5000
1	ABRAMS TESTING SFAE GCSS W AB QT J MORAN 6501 ELEVEN MILE RD WARREN MI 48397-5000
1	COMMANDER WATERVLIET ARSENAL SMCWV QAE Q B VANINA BLDG 44 WATERVLIET NY 12189-4050
2	SFSJM CDL AMMUN TEAM R CRAWFORD W HARRIS 1 ROCK ISLAND ARSENAL ROCK ISLAND IL 61299-6000
1	COMMANDER US ARMY AMCOM AVN APPLIED TECH DIR J SCHUCK FORT EUSTIS VA 23604-5577
1	NVL SURFC WARFARE CTR DAHLGREN DIV CODE G06 DAHLGREN VA 22448
1	USA SBCCOM PM SOLDIER SPT AMSSB PM RSS A J CONNORS KANSAS ST NATICK MA 01760-5057

NO. OF COPIES	ORGANIZATION
3	AIR FORCE ARMAMENT LAB AFATL DLJW W COOK D BELK J FOSTER EGLIN AFB 32542
1 (CD only)	DPTY ASSIST SCY FOR R&T SARD TT ASA (ACT) J PARMENTOLA THE PENTAGON RM E3479 WASHINGTON DC 20310-0103
1	DARPA W COBLENZ 3701 N FAIRFAX DR ARLINGTON VA 22203-1714
1	US ARMY TACOM ARDEC AMSRD AAR AEE W E BAKER BLDG 3022 PICATINNY ARSENAL NJ 07806-5000
11	US ARMY TARDEC AMSTRA TR R MS 263 K BISHNOI D TEMPLETON (10 CPS) WARREN MI 48397-5000
2	CALTECH G RAVICHANDRAN T AHRENS MS 252 21 1201 E CALIFORNIA BLVD PASADENA CA 91125
2	UNIV OF DELAWARE DEPT OF MECH ENGR J GILLESPIE NEWARK DE 19716
5	SOUTHWEST RSRCH INST C ANDERSON K DANNEMANN T HOLMQUIST G JOHNSON J WALKER PO DRAWER 28510 SAN ANTONIO TX 78284

NO. OF COPIES ORGANIZATION

3 SRI INTRNTL
D CURRAN
D SHOCKEY
R KLOOP
333 RAVENSWOOD AVE
MENLO PARK CA 94025

1 APPLIED RSRCH ASSOC
D GRADY
4300 SAN MATEO BLVD NE
STE A220
ALBUQUERQUE NM 87110

1 INTRNTL RSRCH ASSOC INC
D ORPHAL
4450 BLACK AVE
PLEASANTON CA 94566

1 BOB SKAGGS CONSULTANT
S R SKAGGS
7 CAMINO DE LOS GARDUNOS
SANTA FE NM 87506

2 WASHINGTON ST UNIV
INST OF SHOCK PHYSICS
Y GUPTA
J ASAY
PULLMAN WA 99164-2814

1 COORS CERAMIC CO
T RILEY
600 NINTH ST
GOLDEN CO 80401

1 UNIV OF DAYTON
RSRCH INST
N BRAR
300 COLLEGE PARK
MS SPC 1911
DAYTON OH 45469-0168

1 PROJECT MANAGER
ABRAMS TANK SYS
J ROWE
WARREN MI 48397-5000

2 COMMANDER
US ARMY TACOM
AMSTA TR S
T FURMANIAK
L PROKURAT FRANKS
WARREN MI 48397-5000

NO. OF COPIES ORGANIZATION

3 COMMANDER
US ARMY RSRCH OFC
B LAMATINA
D STEPP
W MULLINS
PO BOX 12211
RSRCH TRIANGLE PARK NC
27709-2211

1 NVL SURFC WARFARE CTR
CARDEROCK DIV
R PETERSON
CODE 28
9500 MACARTHUR BLVD
WEST BETHESDA MD 20817-5700

4 LAWRENCE LIVERMORE NATL LAB
R GOGOLEWSKI L290
R LANDINGHAM L369
J E REAUGH L282
S DETERESA
PO BOX 808
LIVERMORE CA 94550

5 SANDIA NATL LAB
J ASAY MS 0548
R BRANNON MS 0820
L CHABILDAS MS 0821
D CRAWFORD ORG 0821
M KIPP MS 0820
PO BOX 5800
ALBUQUERQUE NM 87185-0820

3 RUTGERS
THE STATE UNIV OF NEW JERSEY
DEPT OF CRMCS & MATLS ENGRG
R HABER
607 TAYLOR RD
PISCATAWAY NJ 08854

2 THE UNIV OF TEXAS AT AUSTIN
S BLESS
IAT
3925 W BRAKER LN STE 400
AUSTIN TX 78759-5316

3 SOUTHWEST RSRCH INST
C ANDERSON
J RIEGEL
J WALKER
6220 CULEBRA RD
SAN ANTONIO TX 78238

NO. OF COPIES ORGANIZATION

1 CERCOM
R PALICKA
991 PARK CTR DR
VISTA CA 92083

6 GDLS
W BURKE MZ436 21 24
G CAMPBELL MZ436 30 44
D DEBUSSCHER MZ436 20 29
J ERIDON MZ436 21 24
W HERMAN MZ435 01 24
S PENTESCU MZ436 21 24
38500 MOUND RD
STERLING HTS MI 48310-3200

1 INTRNTL RSRCH ASSN
D ORPHAL
4450 BLACK AVE
PLEASANTON CA 94566

1 JET PROPULSION LAB
IMPACT PHYSICS GROUP
M ADAMS
4800 OAK GROVE DR
PASADENA CA 91109-8099

3 OGARA HESS & EISENHARDT
G ALLEN
D MALONE
T RUSSELL
9113 LE SAINT DR
FAIRFIELD OH 45014

2 CERADYNE INC
M NORMANDIA
3169 REDHILL AVE
COSTA MESA CA 96626

3 JOHNS HOPKINS UNIV
DEPT OF MECH ENGRNG
K T RAMESH
3400 CHARLES ST
BALTIMORE MD 21218

2 SIMULA INC
V HORVATICH
V KELSEY
10016 51ST ST
PHOENIX AZ 85044

NO. OF COPIES ORGANIZATION

3 UNITED DEFNS LTD PARTNERS
GROUND SYS DIV
E BRADY
R JENKINS
K STRITTMATTER
PO BOX 15512
YORK PA 17405-1512

10 NATL INST OF STANDARD & TECH
CRMCS DIV
G QUINN
STOP 852
GAITHERSBURG MD 20899

2 DIR USARL
AMSRD ARL D
C CHABALOWSKI
V WEISS
BLDG 205
2800 POWDER MILL RD
ADELPHI MD 20783-1197

ABERDEEN PROVING GROUND

63 DIR USARL
RDRL SL
R COATES
RDRL WM
S KARNA
J MCCAULEY (20 CPS)
J SMITH
T WRIGHT
RDRL WML
J NEWILL
M ZOLTOSKI
RDRL WML H
T FARRAND
L MAGNESS
D SCHEFFLER
R SUMMERS
RDRL WMM
R DOWDING
RDRL WMM B
G GAZONAS
RDRL WMM D
E CHIN
K CHO
R SQUILLACIOTI

NO. OF
COPIES ORGANIZATION

RDRL WMM E
J LASALVIA
P PATEL
J SANDS
RDRL WMM F
J MONTGOMERY
RDRL WMP
P BAKER
B BURNS
S SCHOENFELD
RDRL WMP B
J CLAYTON
D DANDEKAR
M GREENFIELD
C HOPPEL
M SCHEIDLER
T WEERASOORIYA
RDRL WMP C
T BJERKE
K KIMSEY
S SEGLETES
W WALTERS
RDRL WMP D
T HAVEL
M KEELE
D KLEPONIS
H MEYER
J RUNYEON
RDRL WMP E
P BARTKOWSKI
M BURKINS
W GOOCH
D HACKBARTH
E HORWATH
T JONES

3 FRAUNHOFFER INSTITUT FÜR
KURZZEITDYNAMIK (EMI)
K THOMA
E STRASSBURGER
A KLINGELBERG 1 D 79588
EFRINGEN KIRCHEN
GERMANY